A Dynamic Corral Model of Receptor Trafficking at a Synapse

Paul C. Bressloff* and Berton A. Earnshaw
Department of Mathematics, University of Utah, Salt Lake City, Utah

ABSTRACT The postsynaptic density (PSD) is a cytoskeletal specialization within the postsynaptic membrane of a neuron that helps to concentrate and organize neurotransmitter receptors at a chemical synapse. The total number of receptors within the PSD, which is a major factor in determining the physiological strength or weight of a synapse, fluctuates due to the surface diffusion of receptors into and out of the PSD, and the interactions of receptors with scaffolding proteins and cytoskeletal elements within the PSD. In this article, we present a stochastic model of protein receptor trafficking at the PSD that takes into account these various processes. The PSD is treated as a stochastically gated corral, which contributes a source of extrinsic or environmental noise that supplements the intrinsic noise arising from small receptor numbers. Using a combination of stochastic analysis and Monte Carlo simulations, we determine the time-dependent variation in the mean and variance of synaptic receptor numbers for a variety of initial conditions that simulate fluorescence recovery after photobleaching experiments, and indicate how such data might be used to infer certain properties of the PSD.

INTRODUCTION

Recent fluorescent recovery after photobleaching (FRAP) and single-particle tracking experiments have revealed that neurotransmitter receptors undergo periods of free diffusion within the plasma membrane of a neuron interspersed with periods of restricted motion in confinement domains that coincide with synapses (1–7). This is consistent with the notion that when a receptor flows into a synapse it is temporarily confined through interactions with scaffolding proteins and cytoskeletal elements within the postsynaptic density (PSD), which is the protein-rich region directly apposed to the active zone of the presynaptic terminal (see Fig. 1 *A*). It follows that under basal conditions, the steady-state receptor concentration within a synapse is determined by a dynamical equilibrium in which the various receptor fluxes into and out of the PSD are balanced. Activity-dependent changes of one or more of these fluxes can then modify the number of receptors in the PSD and thus alter the strength or weight of a synapse. Indeed, there is growing experimental evidence that the activity-dependent regulation of receptor trafficking plays an important role in synaptic plasticity (8,9).

The dynamical processes underlying receptor trafficking are stochastic in nature, suggesting that the strength of a synapse will undergo random fluctuations due to activity-independent variations in the number of synaptic receptors. Quantifying such fluctuations is important both for interpreting FRAP experiments and for understanding how synaptic weights can provide a robust subcellular substrate for learning and memory. It is useful to distinguish between two sources of stochasticity: intrinsic noise arising from fluctuations in synaptic receptor number within a fixed environment, which will be significant when the mean number of receptors is small, and extrinsic noise arising from fluctuations of the environment itself. Possible sources of extrinsic noise include dynamical reorganization of transmembrane proteins or submembranous cytoskeletal elements that corral receptors within a synapse, fluctuations in the number of scaffolding proteins, and fluctuations in the background concentration of extrasynaptic receptors.

In a recent model of receptor trafficking, Holcman and Triller (10) analyze the steady-state mean and variance of bound receptors in a PSD as a function of the rates of entry into and exit from the PSD as well as the rates of binding to and unbinding from scaffolding proteins. The entry, exit, binding, and unbinding rates are taken to be fixed so that the variance arises solely from the intrinsic noise associated with small receptor numbers. In this article, we generalize the Holcman and Triller model by incorporating a source of extrinsic noise in the form of a stochastic gate, and calculate the resulting time-dependent and steady-state mean and variance of both free and bound receptors within the PSD. We treat the PSD as a single homogeneous compartment within which receptors exist in one of two states: either bound to scaffolding proteins or unbound and diffusing freely within the PSD. The number of scaffolding protein binding sites is held fixed, as are the binding and unbinding rates. However, the rates of entry and exit are taken to be stochastic variables that fluctuate with the opening and closing of the gate. To determine the steady-state and time-dependent statistics of both free and bound receptors in this extended model, we generalize the analysis of the so-called dynamic corral model due to Brown et al. (11) (see also (12–14)). In the dynamic corral model, proteins diffuse both within and without a homogeneous region called the corral, and the rates at which these proteins enter and exit the corral are taken to be stochastic. In fact, our extension of Holcman and Triller's model (by treating the PSD as stochastically

Submitted October 15, 2008, and accepted for publication December 1, 2008.

*Correspondence: bressloff@math.utah.edu

Editor: Alexander Mogilner.

0006-3495/09/03/1786/17 $2.00

doi: 10.1016/j.bpj.2008.12.3889

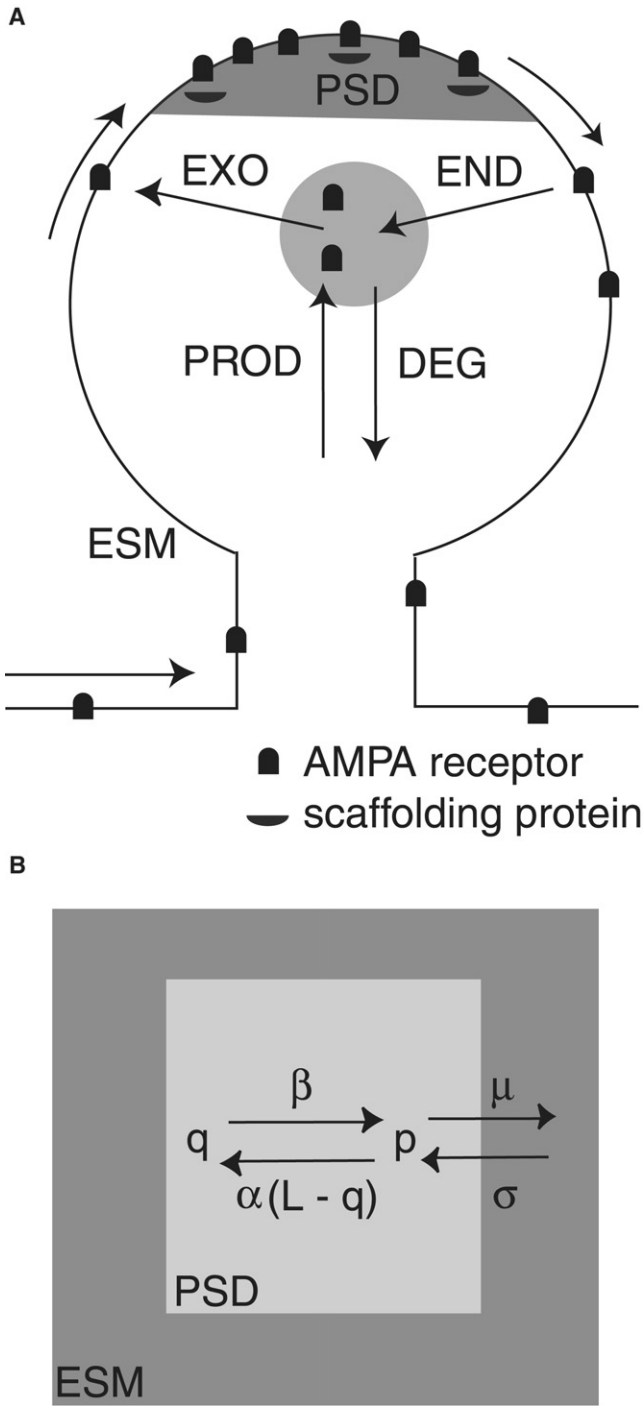

FIGURE 1 (*A*) Schematic illustration of receptor trafficking at the postsynaptic density (*PSD*). In the case of a glutamatergic synapse, the PSD is typically located at the tip or head of a dendritic spine, which is a small, submicrometer membranous extrusion that protrudes from a dendrite. The rest of the membrane of the spine and surrounding dendrite is called the extrasynaptic membrane (*ESM*). Receptors stored in intracellular pools are continually exchanged with surface receptors through exo/endocytosis (*EXO*/*END*) and sorted for degradation (*DEG*). Local production of intracellular receptors can also replenish these pools. Surface receptors enter and exit the PSD via diffusion in the postsynaptic membrane and can be immobilized within the PSD through interactions with scaffolding proteins. It is possible that some intracellular receptors are inserted directly into the PSD, although we ignore that here. (*B*) Schematic representation of Eqs. 1 and 2. Note that although panel *A* illustrates receptor trafficking at PSDs located in dendritic spines, Eqs. 1 and 2 apply equally well to receptor trafficking at PSDs occurring in the dendrite itself, in which case the ESM refers not to the extrasynaptic membrane of the spine head but to the dendritic membrane surrounding the PSD.

gated) is also an extension of the dynamic corral model in that proteins within the corral can now bind to and unbind from sites within the corral. It turns out that our analysis of the extended dynamic corral model is only valid in two distinct trafficking regimes: one in which most binding sites are unoccupied (termed the ''unsaturated regime'') and the other when most binding sites are occupied (termed the ''saturated regime''). Therefore, we supplement our stochastic analysis with Monte Carlo simulations, which are used to determine the time-dependent variation in the mean and variance of free, bound, and total synaptic receptor numbers for a variety of parameter values and initial conditions that simulate FRAP-like experiments. We show that a stochastic gate can have a significant effect on the dynamics of receptor trafficking, often increasing the variance of receptor numbers dramatically and, conversely, binding/unbinding to scaffolding proteins can have a significant effect on the behavior of a dynamic corral.

We note that in Holcman and Triller's model (10) the boundary of the PSD is considered to be impermeable except for a collection of small holes through which receptors can enter and exit. Treating the PSD in this way may account for how adhesion proteins like *N*-cadherin, which occur at the periphery of the PSD, may act like pickets preventing the passage of receptors into and out of the PSD except where these proteins are not sufficiently clustered (15,16). Under this representation of the PSD, fluctuations in the position of these picketlike proteins may provide a physiological representation of our proposed stochastic gate, since one might imagine that such fluctuations cause the small holes to transiently appear and disappear. However, Holcman and Triller's model does not require the boundary of the PSD to be represented in this way; in fact, the existence of small holes is only used to calculate the mean dwell time of a receptor in the PSD (see, e.g., (17,18)) but this calculation is not required for their analysis. Hence, Holcman and Triller's model and our extension of it are generic in the sense that there may be many factors that determine the rates of entry and exit, and each of these factors may themselves be sources of additional extrinsic noise. As an example of another such factor, submembranous structures like the actin cytoskeleton interact with the cytoplasmic tails of the subunits comprising some receptors, and these interactions often confine these receptors within the PSD (15,16). One might imagine, therefore, that fluctuations in the composition of these structures could give rise to the gating mechanism we are proposing. The main point to emphasize here is that treating the PSD as stochastically gated is a plausible way of generically introducing extrinsic noise into the model of Holcman and Triller.

DYNAMIC CORRAL MODEL WITH BINDING

Experimental estimates for the diffusivity D of receptors in the PSD ranges from 0.01 to 0.1 $\mu m^2\ s^{-1}$ (4). Given that the typical length-scale of a synapse is $\ell = 0.1\ \mu m$, it follows that the timescale ℓ^2/D for diffusion within the PSD is 0.1–1 s, which is faster than other transport processes such as binding and unbinding. Ultrastructural studies of the PSD suggest that it is a heterogeneous structure (19). For example, in the case of glutamatergic synapses, different classes of receptor appear to be clustered in different regions of the PSD with NMDA receptors at the center and AMPA receptors in the periphery. We will ignore such fine structure here and treat the PSD as a homogeneous compartment with a spatially uniform distribution of receptors and scaffolding protein binding sites. Let p denote the mean number of freely diffusing receptors within the PSD and q denote the mean number of bound receptors. We can then model receptor dynamics within the PSD according to this pair of kinetic equations:

$$\frac{dp}{dt} = -\alpha(L-q)p + \beta q - \mu p + \sigma, \tag{1}$$

$$\frac{dq}{dt} = \alpha(L-q)p - \beta q. \tag{2}$$

Here L is the number of binding sites within the PSD, α is the particle binding rate per unoccupied binding site, β is the unbinding rate of particles, σ is the number of extrasynaptic receptors entering the PSD per unit time, and μ is the escape rate of free receptors within the PSD. (See Fig. 1 *B* for a schematic representation of Eqs. 1 and 2.) In the case of constant parameters, we have $(p(t),q(t)) \to (\overline{p},\overline{q})$ as $t \to \infty$, where

$$\overline{p} = \frac{\sigma}{\mu}, \quad \overline{q} = \frac{\alpha L \overline{p}}{\alpha \overline{p} + \beta} \tag{3}$$

are the steady-state particle numbers.

Single-particle tracking data suggests that as much as half of the AMPA receptors within a glutamatergic synapse exhibit confined diffusion within the PSD and are thus mobile (4). However, certain care must be taken in identifying mobile and immobile receptors with bound and unbound receptors, respectively, since it is possible that a receptor/scaffolding protein complex could also be partially mobile within the PSD (15). Another important issue concerning the distinction between bound and unbound receptors is to what extent each receptor class contributes to the synaptic current induced by the release of neurotransmitter from the presynaptic terminal, and hence the synaptic weight. It is often assumed that the predominant contribution arises from bound receptors (10). However, activation of extrasynaptic receptors also generates a current, suggesting that a receptor does not have to be bound to a scaffolding protein to act as an ion channel gate. On the other hand, there is growing evidence that receptors form complexes with other proteins that modify channel properties. One well-known example is the binding of AMPA receptors to transmembrane AMPA receptor regulatory proteins such as stargazin (20). Stargazin modulates the gating of AMPA receptors by increasing the rate of channel opening (21). Interestingly, it also contributes to receptor trafficking by facilitating the surface delivery of receptors and by binding to the PDZ-domain-containing protein PSD-95, a major scaffolding protein of the PSD (22). Hence, it is possible that both free and bound receptors contribute to the strength of a synapse, but with different weightings. Here we will simply identify synaptic strength with the total number of receptors within the PSD.

It remains for us to specify the form of the source term σ in Eq. 1. In addition to the lateral movement of receptors within the plasma membrane, there is a continual exchange of surface receptors with intracellular pools known as constitutive recycling. This has been found both for excitatory AMPA receptors (23–25) and inhibitory GABA receptors (26,27). During constitutive recycling, receptors diffuse laterally from the PSD to extrasynaptic sites where they undergo clathrin-dependent endocytosis; internalized receptors are then either sorted to lysosomes for degradation or recycled to the surface. It is currently unclear whether receptors are reinserted directly into the PSD or at extrasynaptic sites, although it is likely that this will depend on the particular type of receptor (see, for example, (28,29)). In our single corral model of the PSD, we will assume that receptors are inserted into the surface extrasynaptically so that the only contribution to the source term σ is from lateral membrane diffusion. As a further simplification, we assume that the background concentration of extrasynaptic receptors is fixed such that $\sigma = C\mu$, where C is a constant. It then follows that for a constant escape rate μ, the steady-state number of free receptors in the PSD is $\overline{p} = C$. Note that elsewhere we have developed a multisynapse model of receptor trafficking, in which the extrasynaptic receptor concentration is determined dynamically by solving an associated reaction-diffusion equation (30). Such a model couples the lateral membrane diffusion of receptors along a dendrite with the internal dynamics of receptor trafficking at a synapse, including constitutive recycling and binding to scaffolding proteins. (In the particular case of AMPA receptors, it is also necessary to take account of the fact that the PSD of a glutamatergic synapse is typically located at the tip or head of a dendritic spine, which is a small, submicrometer membranous protrusion of the dendritic membrane. That is, the PSD couples to the dendrite indirectly via the extrasynaptic membrane of the spine, which can be treated as a second homogeneous compartment (31); and see Fig. 1 *A*.)

The simple PSD model given by Eqs. 1 and 2 represents receptor dynamics in terms of a system of kinetic equations describing the temporal variation of the mean number of bound and unbound receptors within the PSD. However, the number of receptors within a typical synapse can vary

between zero and a few hundred (32), suggesting that random fluctuations about the mean receptor number could be significant. (Roughly speaking, the size of fluctuations relative to the mean number of receptors N varies as $1/\sqrt{N}$.) For fixed values of the various trafficking parameters, these fluctuations reflect the inherent stochasticity or intrinsic noise of receptor trafficking. In addition to intrinsic noise, there can be a number of extrinsic noise sources arising from fluctuations in one or more trafficking parameters, including the number of binding sites L and the extrasynaptic receptor concentration C. As discussed in the Introduction, we will focus on a generic source of extrinsic noise, namely fluctuations in source term σ and the escape rate μ. More specifically, we incorporate the dynamic corral model of Brown et al. (11) by assuming that the escape of a receptor from the PSD is controlled by a stochastic gate that can be in two states, an open state for which $\mu(t) = \mu_o > 0$ and a closed state for which $\mu(t) = \mu_c = 0$. The opening and closing of the stochastic gate is governed by the rate equations

$$\begin{aligned} \frac{d\mathcal{P}^\circ}{dt} &= -\gamma_- \mathcal{P}^\circ + \gamma_+ \mathcal{P}^c \\ \frac{d\mathcal{P}^c}{dt} &= \gamma_- \mathcal{P}^\circ - \gamma_+ \mathcal{P}^c \end{aligned}, \tag{4}$$

where $\mathcal{P}^\circ(t)$ ($\mathcal{P}^c(t)$) is the probability that the gate is open (closed) at time t, and $\gamma_\pm$ are the transition rates between the two states. Thus, the time-dependent escape rate $\mu(t)$ describes a dichotomous noise process. The rate at which receptors enter the PSD is then taken to be $\sigma(t) = C\mu(t)$ with C fixed. As noted in the Introduction, one possible interpretation of the stochastic gate is that it represents the random opening and closing of a small hole within the boundary of the PSD (10,17,18). This suggests that one could consider a multistate version of the stochastic gate, which corresponds to the random opening and closing of multiple small holes within the PSD boundary. In this article, however, we will focus on the simplest case of a two-state stochastic gate.

We now formulate a stochastic version of Eqs. 1 and 2 that accounts for fluctuations in receptor numbers due to both intrinsic noise (i.e., small receptor numbers) and fluctuations in the boundary of the PSD (i.e., $\mu(t)$ follows the two-state Markov process of Eq. 4). Let $P_{n,m}(t)$ denote the probability that there are n free and m bound particles within the PSD at time t. Given the various kinetic processes occurring in Eqs. 1 and 2, it follows that the probability distribution evolves according to the master equation

$$\begin{aligned} \frac{dP_{n,m}}{dt} &= \sigma(t)P_{n-1,m} + \mu(t)(n+1)P_{n+1,m}(t) \\ &\quad - [\sigma(t) + \mu(t)n]P_{n,m} + \alpha(n+1)[L-(m-1)] \\ &\quad \times P_{n+1,m-1}(t) + \beta(m+1)P_{n-1,m+1}(t) \\ &\quad - [\alpha n(L-m) + \beta m]P_{n,m}(t), \end{aligned} \tag{5}$$

with $n \geq 0, L \geq m \geq 0$ and $\sigma(t) = C\mu(t)$. The positive terms represent the various transitions into the state (n, m) whereas the negative terms represent the various transitions from the state (n, m). We take the initial condition to be $P_{n,m}(0) = \delta_{n,n_0}\delta_{m,m_0}$; i.e., at time $t = 0$, there are n_0 free and m_0 bound particles within the PSD. In the case of a static PSD model (i.e., when $\mu(t)$ is constant in time), Eq. 5 reduces to Holcman and Triller's model of receptor trafficking (10). On the other hand, if $\alpha = \beta = 0$ (no binding/unbinding) and $\mu(t)$ evolves according to Eq. 4, then Eq. 5 reduces to the dynamic corral model of Brown et al. (11). Note that when the PSD boundary is fluctuating, we think of the term μ in Eq. 5 as being a single realization of the process described in Eq. 4. As a consequence, different realizations of μ will yield different probability distributions $P_{n,m}$.

ANALYSIS OF MODEL

The analysis of Eq. 5 is nontrivial due to the stochastic nature of the gating parameter $\mu(t)$ and due to the nonlinear reaction rate $\alpha(L-m)n$ for binding to scaffolding proteins. Therefore, we will proceed by considering two distinct approximation schemes, both of which allow us to carry out averaging with respect to the stochastic gating dynamics based on an extension of Brown et al. (11) to the multivariate case. The first scheme involves a linearization of the binding reaction rate under the assumption that the binding sites are unsaturated, that is, $m(t) << L$ for all t (such a regime arises when $\alpha n(t) << \beta$). The resulting master equation can then be analyzed using generating functions. In the second scheme we assume that the binding sites are saturated, that is, $m(t) = L$ for all t (such a regime arises when $\alpha n(t) >> \beta$). This effectively eliminates the dynamics of bound receptors from the model, and we are left with the master equation considered in Brown et al. (11).

Unsaturated binding sites: linearized reaction rates and generating functions

Suppose that we linearize the reaction rates in Eq. 5 by making the approximation $\alpha(L-m)n \approx \alpha Ln$, which as we noted above is valid when the binding sites are unsaturated (when $m << L$). Note that this approximation is exact in the limit $L \to \infty$ while holding αL fixed (i.e., if $L \to \infty$ then $m << L$ for all m). It is important to note that while holding αL fixed in this limit requires the binding rate per unoccupied binding site α to go to zero, in practice this means that as long as $m << L$ only the product αL is relevant, not the individual values of α and L.

Introducing the generating function

$$G(u, v, t) = \sum_{n=0}^{\infty}\sum_{m=0}^{\infty} u^n v^m P_{n,m}(t), \tag{6}$$

one obtains from Eq. 5 (after applying to Eq. 5 the limit $L \to \infty$ holding αL fixed) the first-order linear partial differential equation for G,

$$\frac{\partial G}{\partial t} + [\mu(t)(u-1) + \alpha L(\mu - v)]\frac{\partial G}{\partial u} - \beta(u-v)\frac{\partial G}{\partial v} = \sigma(t)(u-1)G, \quad (7)$$

with initial condition $G(u,v,0) = u^{n_0}v^{m_0}$ (as expected, α and L appear in Eq. 7 only as the product αL). Equation 7 can be solved using the method of characteristics (33), which we do in Appendix A. The solution is

$$G(u,v,t) = f_1(u,v,t)^{n_0} f_2(u,v,t)^{m_0} \mathrm{e}^{\Lambda_u(t)(u-1)} \mathrm{e}^{\Lambda_v(t)(v-1)}, \quad (8)$$

where

$$f_i(u,v,t) = 1 + \mathcal{N}_{i1}(t)(u-1) + \mathcal{N}_{i2}(t)(v-1) \quad (i = 1,2) \quad (9)$$

and

$$\Lambda_u(t) = C\left(1 - \mathcal{N}_{11}(t) - \frac{\alpha L}{\beta}\mathcal{N}_{21}(t)\right), \quad (10)$$

$$\Lambda_v(t) = C\left(\frac{\alpha L}{\beta} - \mathcal{N}_{12}(t) - \frac{\alpha L}{\beta}\mathcal{N}_{22}(t)\right). \quad (11)$$

Here $\mathcal{N}_{ij}$ is the ij^{th} entry of the matrix $\mathcal{N}$ defined according to

$$\mathcal{N}(t) = \exp\left(-\int_0^t \mathcal{M}(t')dt'\right),$$
$$\mathcal{M}(t) = \begin{pmatrix} \mu(t) + \alpha L & -\alpha L \\ -\beta & \beta \end{pmatrix}; \quad (12)$$

see also Eq. 38.

Equations 8–11 allow us to calculate the mean and variance of n (number of free receptors), m (number of bound receptors), and $N = n + m$ (total number of receptors) via the formulae

$$E_\mu(n) = \left.\frac{\partial G}{\partial u}\right|_{u=v=1}, \; E_\mu(m) = \left.\frac{\partial G}{\partial v}\right|_{u=v=1}$$
$$E_\mu(n^2 - n) = \left.\frac{\partial^2 G}{\partial u^2}\right|_{u=v=1}, \; E_\mu(m^2 - m) = \left.\frac{\partial^2 G}{\partial v^2}\right|_{u=v=1},$$
$$E_\mu(nm) = \left.\frac{\partial^2 G}{\partial v \partial u}\right|_{u=v=1}$$

where the subscript μ indicates that these means are calculated with respect to a single realization of the random variable μ only, and may therefore take on different values for different realizations of μ. Calculating these derivatives yields

$$E_\mu(n) = C + (n_0 - C)\mathcal{N}_{11} + (m_0 - C\alpha L/\beta)\mathcal{N}_{21}, \quad (13)$$

$$E_\mu(m) = C\alpha L/\beta + (n_0 - C)\mathcal{N}_{12} + (m_0 - C\alpha L/\beta)\mathcal{N}_{22}, \quad (14)$$

$$E_\mu(N) = E_\mu(n) + E_\mu(m), \quad (15)$$

and

$$\mathrm{Var}_\mu(n) = E_\mu(n) - n_0(\mathcal{N}_{11})^2 - m_0(\mathcal{N}_{21})^2, \quad (16)$$

$$\mathrm{Var}_\mu(m) = E_\mu(m) - n_0(\mathcal{N}_{12})^2 - m_0(\mathcal{N}_{22})^2, \quad (17)$$

$$\mathrm{Var}_\mu(N) = \mathrm{Var}_\mu(n) + \mathrm{Var}_\mu(m) - 2(n_0\mathcal{N}_{11}\mathcal{N}_{12} + m_0\mathcal{N}_{21}\mathcal{N}_{22}), \quad (18)$$

where we have omitted any t-dependence for notational convenience. Note that the variance in the total number of receptors is not simply the sum of the variances of the bound and unbound receptor numbers because the two receptor states co-vary. In the case $n_0 = m_0 = 0$ (zero receptors in the PSD at $t = 0$), the generating function defined by Eq. 8 reduces to the product of two Poissonian generating functions of mean Λ_u and Λ_v, respectively, implying that the joint distribution of free and bound particle numbers decomposes into the product of two time-dependent Poissonian distributions,

$$P_{n,m}(t) = \frac{\mathrm{e}^{-\Lambda_u(t)}\Lambda_u(t)^n}{n!}\frac{\mathrm{e}^{-\Lambda_v(t)}\Lambda_v(t)^m}{m!}$$

and Eqs. 13–18 simplify to

$$E_\mu(n) = \mathrm{Var}_\mu(n) = \Lambda_u,$$
$$E_\mu(m) = \mathrm{Var}_\mu(m) = \Lambda_v,$$
$$E_\mu(N) = \mathrm{Var}_\mu(N) = \Lambda_u + \Lambda_v.$$

To obtain a more useful characterization of the means and variances given in Eqs. 13–18, we average over all possible stochastic realizations of the gate along lines analogous to the scalar case considered in Brown et al. (11). As was noted previously, when the PSD gate is fluctuating, the solution $P_{n,m}$ of Eq. 5 depends on the particular realization of μ chosen. Each realization μ is itself drawn from a distribution of realizations evolving according to Eq. 4, and it is with respect to this distribution that we are averaging. Formally denoting this average over realizations of μ by $\langle \ldots \rangle$, we obtain

$$E(n) \equiv \langle E_\mu(n) \rangle = C + (n_0 - C)\langle \mathcal{N}_{11} \rangle + (m_0 - C\alpha L/\beta)\langle \mathcal{N}_{21} \rangle, \quad (19)$$

$$E(m) \equiv \langle E_\mu(m) \rangle = C\alpha L/\beta + (n_0 - C)\langle \mathcal{N}_{12} \rangle + (m_0 - C\alpha L/\beta)\langle \mathcal{N}_{22} \rangle, \quad (20)$$

$$E(N) \equiv \langle E_\mu(N) \rangle = E(n) + E(m), \quad (21)$$

and

$$\mathrm{Var}(n) \equiv \langle E_\mu(n^2) \rangle - \langle E_\mu(n) \rangle^2 = E(n) - n_0\langle (\mathcal{N}_{11})^2 \rangle - m_0\langle (\mathcal{N}_{21})^2 \rangle + (n_0 - C)^2\left(\langle (\mathcal{N}_{11})^2 \rangle - \langle \mathcal{N}_{11} \rangle^2\right) + (m_0 - C\alpha L/\beta)^2\left(\langle (\mathcal{N}_{21})^2 \rangle - \langle \mathcal{N}_{21} \rangle^2\right) + (n_0 - C)(m_0 - C\alpha L/\beta)(\langle \mathcal{N}_{11}\mathcal{N}_{21} \rangle - \langle \mathcal{N}_{11} \rangle \langle \mathcal{N}_{21} \rangle), \quad (22)$$

$$\begin{aligned}\mathrm{Var}(m) \equiv \langle E_\mu(m^2)\rangle - \langle E_\mu(m)\rangle^2 = {} & E(m) - n_0\langle(\mathcal{N}_{12})^2\rangle \\ & - m_0\langle(\mathcal{N}_{22})^2\rangle + (n_0 - C)^2\big(\langle(\mathcal{N}_{12})^2\rangle \\ & - \langle\mathcal{N}_{12}\rangle^2\big) + (m_0 - C\alpha L/\beta)^2\big(\langle(\mathcal{N}_{22})^2\rangle \\ & - \langle\mathcal{N}_{22}\rangle^2\big) + (n_0 - C)(m_0 - C\alpha L/\beta) \\ & \times (\langle\mathcal{N}_{12}\mathcal{N}_{22}\rangle - \langle\mathcal{N}_{12}\rangle\langle\mathcal{N}_{22}\rangle), \end{aligned} \tag{23}$$

$$\begin{aligned}\mathrm{Var}(N) \equiv \langle E_\mu(N^2)\rangle - \langle E_\mu(N)\rangle^2 = {} & \mathrm{Var}(n) + \mathrm{Var}(m) \\ & - 2(n_0\langle\mathcal{N}_{11}\mathcal{N}_{12}\rangle + m_0\langle\mathcal{N}_{21}\mathcal{N}_{22}\rangle) \\ & + 2(n_0 - C)^2(\langle\mathcal{N}_{11}\mathcal{N}_{12}\rangle - \langle\mathcal{N}_{11}\rangle\langle\mathcal{N}_{12}\rangle) \\ & + 2(m_0 - C\alpha L/\beta)^2(\langle\mathcal{N}_{21}\mathcal{N}_{22}\rangle - \langle\mathcal{N}_{21}\rangle\langle\mathcal{N}_{22}\rangle) \\ & + 2(n_0 - C)(m_0 - C\alpha L/\beta)(\langle\mathcal{N}_{11}\mathcal{N}_{22}\rangle \\ & - \langle\mathcal{N}_{11}\rangle\langle\mathcal{N}_{22}\rangle) + 2(n_0 - C)(m_0 - C\alpha L/\beta) \\ & \times (\langle\mathcal{N}_{21}\mathcal{N}_{12}\rangle - \langle\mathcal{N}_{21}\rangle\langle\mathcal{N}_{12}\rangle). \end{aligned} \tag{24}$$

Evaluating the averages $\langle\mathcal{N}_{ij}\rangle$, $\langle\mathcal{N}_{ij}\mathcal{N}_{kl}\rangle$, and $\langle\mathcal{N}_{i1}\mathcal{N}_{j2}\rangle$ can be performed using a method originally developed by Kubo (34) in the study of spectral line broadening in a quantum system, and subsequently extended to chemical rate processes with dynamical disorder by Zwanzig (35). The details of these calculations for the averages $\langle\mathcal{N}_{ij}\rangle$ and $\langle\mathcal{N}_{ij}\mathcal{N}_{kl}\rangle$ are given in Appendix B while the details for the calculation of $\langle\mathcal{N}_{i1}\mathcal{N}_{j2}\rangle$ can be found in Appendix C. One can verify from these calculations that each of these averages approaches zero as time increases, hence the steady-state means and variances in the unsaturated regime are

$$E_\infty(n) = \mathrm{Var}_\infty(n) = C, \tag{25}$$

$$E_\infty(m) = \mathrm{Var}_\infty(m) = C\alpha L/\beta, \tag{26}$$

$$E_\infty(N) = \mathrm{Var}_\infty(N) = C(1 + \alpha L/\beta). \tag{27}$$

Saturated binding sites: corral model of Brown et al.

At the other extreme, we now assume that $m(t) = L$ for all t. From Eq. 3 we see that the mean steady-state value $\overline{q}$ of m is approximately L only when $\alpha\,\overline{p} >> \beta$, hence we expect the approximation $m(t) = L$ to be valid only when $\alpha n(t) >> \beta$. In such a regime, the timescale associated with unbinding is orders-of-magnitude larger than that associated with binding, hence whenever a bound receptor unbinds, the binding site it leaves unoccupied is rapidly occupied by a free receptor. In the limit that this exchange is instantaneous, an unbinding event produces no change in either free or bound receptor numbers, effectively eliminating the dynamics of the bound receptors. Therefore, the probability distribution P_n for the number of free receptors n evolves according to the simplified master equation

$$\frac{dP_n}{dt} = \mu(t)[CP_{n-1} + (n+1)P_{n+1}(t) - (C+n)P_n], \tag{28}$$

where we have already employed the relationship $\sigma(t) = C\mu(t)$. This is precisely the master equation studied by Brown et al. (11) for the dynamics of a freely diffusing particle in an isolated, stochastically gated corral. It therefore follows from their work that by setting

$$w(t) = \exp\left(-\int_0^t \mu(t')dt'\right),$$

we have

$$E_\mu(n) = (n_0 - C)w + C,\ E_\mu(N) = E_\mu(n) + L, \tag{29}$$

$$\mathrm{Var}_\mu(n) = E_\mu(n) - n_0w^2,\ \mathrm{Var}_\mu(N) = \mathrm{Var}_\mu(n), \tag{30}$$

and

$$E(n) = (n_0 - C)\langle w\rangle + C, \quad E(N) = E(n) + L, \tag{31}$$

$$\mathrm{Var}(n) = E(n) - n_0\langle w^2\rangle + (n_0 - C)^2\big(\langle w^2\rangle - \langle w\rangle^2\big), \tag{32}$$

$$\mathrm{Var}(N) = \mathrm{Var}(n), \tag{33}$$

where

$$\langle w(t)^j\rangle = \begin{pmatrix}1\\1\end{pmatrix}^T \exp\left[-t\begin{pmatrix}j\mu_o + \gamma_- & -\gamma_+\\ -\gamma_- & \gamma_+\end{pmatrix}\right] \times \begin{pmatrix}\Pi_o\\ \Pi_c\end{pmatrix}, \quad (j = 1, 2).$$

Here Π_l, $l = o, c$, are the stationary probability distributions for the dichotomous noise process of Eq. 4:

$$\Pi_o = \frac{\gamma_+}{\gamma_+ + \gamma_-}, \quad \Pi_c = \frac{\gamma_-}{\gamma_+ + \gamma_-}.$$

It is important to note that since $m(t)$ is always L, its mean is L and variance is zero. The averages $\langle w^j\rangle$, $j = 1, 2$, approach zero as time increases, hence the steady-state means and variances are

$$E_\infty(n) = \mathrm{Var}_\infty(n) = C, \tag{34}$$

$$E_\infty(N) = C + L,\ \mathrm{Var}_\infty(N) = C. \tag{35}$$

RESULTS

In this section we use the analytical expressions for the mean and variance of receptor numbers derived in the previous section, along with Monte Carlo simulations of the master equation from Eq. 5 in cases where our analytical approximations are not valid, to investigate the stochastic dynamics of receptor trafficking within the PSD. In particular, we determine how fluctuations in receptor number depend on the rates of receptor binding/unbinding and the dynamics of the stochastic gate. We highlight differences in behavior that arise when the PSD operates in either a saturated or an unsaturated regime, and when the effective rate of escape

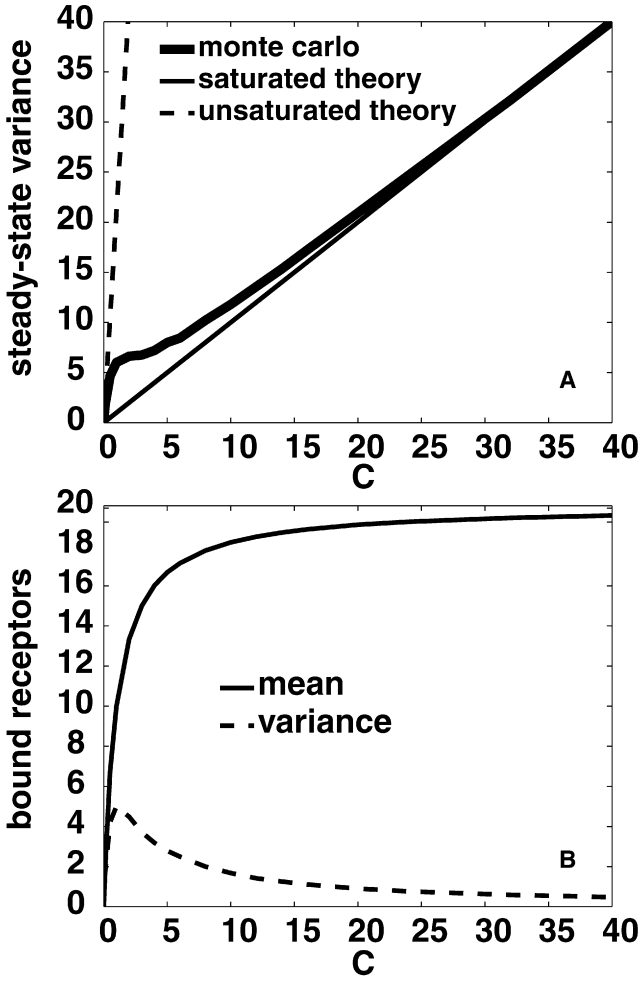

FIGURE 2 Steady-state trafficking of synaptic receptors. (*A*) Variance in the total receptor number as a function of C for $\alpha = \beta = 10^{-3}\ s^{-1}$, $L = 20$. Note that the steady-state statistics do not depend on gate dynamics. Monte Carlo simulations (*thick solid*) are compared with predictions for a saturated (*thin solid*) and unsaturated (*dashed*) PSD. As C increases, the PSD transitions from being unsaturated to being saturated. (*B*) Steady-state mean (*solid*) and variance (*dashed*) of the bound receptor number as a function of C. These values were obtained from the Monte Carlo simulation of *A*. The variance is initially equal to the mean while the PSD is unsaturated, but as C increases the PSD becomes saturated and the variance decays back to zero. Compare to Fig. 2 of Holcman and Triller (10).

through the stochastic gate is either slow or fast compared to the rates of binding/unbinding. Using our model to characterize fluctuations across a wide range of parameter regimes is particularly useful given that the detailed biophysical properties of corrals and other confining structures within the PSD have not yet been determined experimentally. It is also difficult to specify the values of the binding/unbinding rates, since they are likely to take on a range of values, from seconds to hours, depending on the configurational state of the receptor (10,31).

Another motivation for our study is to determine how inclusion of binding and unbinding into the dynamic corral model of Brown et al. (11) modifies the time-dependent statistics of protein fluctuations. When we wish to compare our results with those of Brown et al. (11), we will take the gating parameters proposed in that article: $\gamma_+ = 20\ s^{-1}$, $\gamma_- = 320\ s^{-1}$, and $\mu_o = 300\ s^{-1}$. (We remind the reader that γ_+ and γ_- are the opening and closing rates of the stochastic gate, respectively, and that μ_o is the escape rate of receptors when the gate is open.) Brown et al. choose the closing rate γ_- to be an order-of-magnitude larger than the opening rate γ_+ so that the corral spends enough time in the closed state between gate openings to allow receptors to redistribute uniformly via diffusion, consistent with our treatment of the PSD as a uniform compartment. When the gate is not fluctuating, we also follow Brown et al. and take the static escape rate μ to be the following function of $\gamma_\pm$ and μ_o:

$$\mu = \frac{\gamma_+ + \gamma_- + \mu_o}{2}\left(1 - \sqrt{1 - \frac{4\mu_o\gamma_+}{(\gamma_+ + \gamma_- + \mu_o)^2}}\right). \tag{36}$$

Doing so ensures that the time course of the mean number of receptors is the same in both the static and stochastic cases, regardless of the particular values of $\gamma_\pm$ and μ_o (see (12) for an explanation of this expression). For the values of $\gamma_\pm$ and μ_o mentioned above, we find that $\mu \approx 9.52\ s^{-1}$. It should be remembered that the gate parameters of Brown et al. (11) were not chosen with receptor trafficking at a PSD in mind, hence these rates do not necessarily reflect those that might be measured at an actual PSD; nevertheless, using these values allows us to make clear how our model extends the dynamic corral model.

Finally, we mention that all Monte Carlo simulations were performed by computing the statistics of a large number (10,000–50,000) of stochastic realizations of Eq. 5, each of which was obtained using the Gillespie algorithm (36). This method of Monte Carlo simulation is known to be exact in the limit where the number of realizations becomes large.

Fluctuations in the steady state

Let us begin by considering the mean and variance of receptor numbers in the steady state. In Fig. 2 *A* we plot, using Monte Carlo simulations, the steady-state variance in the total number of receptors as a function of the steady-state mean number of free receptors C in the case of a static gate with $\alpha = \beta = 10^{-3}\ s^{-1}$, $L = 20$. Also shown is the variance predicted by both our unsaturated and saturated theory, as given in Eqs. 27 and 35, respectively. In Fig. 2 *B*, we plot using Monte Carlo simulations the corresponding mean and variance of bound receptors as a function of C. We remark that the Monte Carlo simulations were performed with a static gate; however, performing these simulations with a stochastic gate would give the same steady-state mean and variance provided that the stochastic gating parameters are related to the static escape rate μ according to

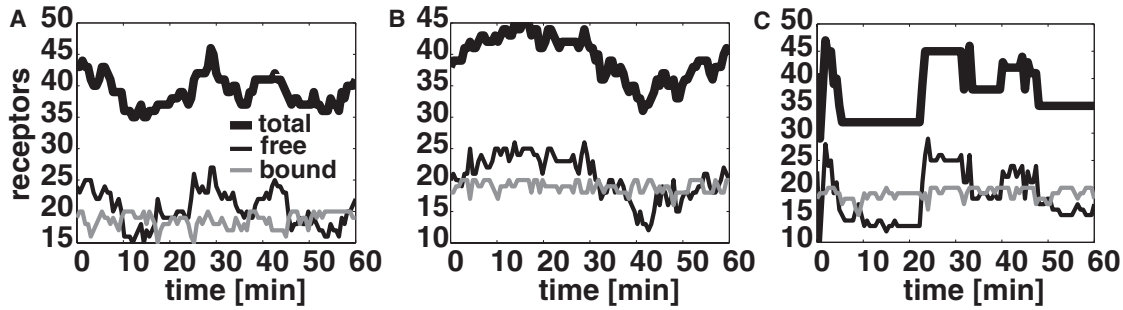

FIGURE 3 Steady-state trajectories illustrating temporal fluctuations in the number of receptors for $C = 20$ and other parameters as in Fig. 2. (*A*) Static gate with escape rate $\mu = 10^{-3}$ s^{-1}. (*B*) Dynamic gate with fast switching. Gating variables are $\gamma_+ = 0.1$ s^{-1}, $\gamma_- = 1$ s^{-1}, and $\mu_o = 0.0111$ s^{-1}. (*C*) Dynamic gate with slow switching. Gating variables are $\gamma_+ = 0.0011$ s^{-1}, $\gamma_- = 0.011$ s^{-1}, and $\mu_o = 0.1110$ s^{-1}.

Eq. 36. When C is small ($C \leq 1$), the PSD is in an unsaturated state, hence the total number of PSD receptors follows our unsaturated approximation and the variance in bound receptors is equal to the mean number of bound receptors. However, as C gets larger there is a clear transition of the PSD from an unsaturated to a saturated state: the variance in the total receptor number approaches our saturated approximation, and the variance in the bound number of receptors decays to zero.

Note that Holcman and Triller (10) carry out a similar steady-state analysis of the master equation, Eq. 5, for a static gate. However, their approach to solving Eq. 5 differs from ours in that they do not consider saturated and unsaturated regimes, but instead assume that the unbinding rate β is much faster than both the binding rate α and the escape rate μ. They also assume that the entry rate σ is large. These assumptions assure that most of the receptors found in the PSD are free, which allows the authors to approximate the mean and variance of bound receptor numbers by decoupling the dynamics of receptor entry and exit from the dynamics of receptor binding and unbinding. As a consequence, their approximations are valid over a wide range of values of C, not just those that put the PSD in either a saturated or unsaturated regime. In fact, although Holcman and Triller do not provide a comparison of their results with Monte Carlo simulations, we report here that their approximations for the steady-state mean and variance of bound receptor numbers (see (10), Eqs. 10 and 11 and Fig. 2) agree well with the Monte Carlo simulation shown in Fig. 2 *B*, especially for larger values of C.

In Fig. 3 we show single stochastic realizations of the number of PSD receptors in steady-state for a static gate (*A*), a stochastic gate with fast switching (*B*), and a stochastic gate with slow switching (*C*). The escape rate for the static gate is $\mu = 10^{-3}$ s^{-1}, whereas the gating variables for the fast gate are $\gamma_+ = 0.1$ s^{-1}, $\gamma_- = 1$ s^{-1}, and $\mu_o = 0.0111$ s^{-1}; and for the slow gate we take $\gamma_+ = 0.0011$ s^{-1}, $\gamma_- = 0.011$ s^{-1}, and $\mu_o = 0.1110$ s^{-1}. This particular value of μ is representative of the escape rates we have used in previous studies of receptor trafficking (see, e.g., (31)). The rates $\gamma_\pm$ are chosen arbitrarily except that γ_- is taken to be an order-of-magnitude larger than γ_+ in order that our treatment of the PSD as a homogeneous compartment be valid (see beginning of this section). The escape rate μ_o is then determined from Eq. 36 so that the dynamic and static gates produce the same steady-state first-order statistics. Other parameter values are as in Fig. 2, with $C = 20$. Although the choice $C = 20$ puts the PSD in a nearly saturated regime, bound receptor numbers still fluctuate throughout the simulations, mainly in response to large fluctuations in the number of free receptors. One interesting observation is that although the steady-state mean and variance of the total number of receptors is the same for the three examples shown in Fig. 3, there are clear differences in the trajectory of the slow stochastic gate compared to the static and fast stochastic gates. That is, in the case of the slow gate there are long time intervals over which the gate is closed, so that the total number of synaptic receptors does not change. To extract such behavior analytically it would be necessary to consider higher-order statistics such as two-point correlation functions.

Relaxation to the steady state: simulating FRAP and inverse FRAP experiments

Significant differences between a static and a stochastic gate arise when the PSD is not in steady state, as we demonstrate for a variety of FRAP and inverse FRAP-like simulations (see Fig. 4 for a schematic illustration of FRAP and inverse FRAP experiments). Before we begin, in Fig. 5 we determine how well our time-dependent analytical approximations for the mean and variance of total receptor numbers in the saturated and unsaturated regimes agree with the mean and variance obtained by Monte Carlo simulation of an extension of the master equation, Eq. 5, that tracks both bleached and unbleached receptors. This extended master equation is comprised of two copies of Eq. 5, one for bleached receptors and the other for unbleached receptors, with modifications that account for the fact that both kinds of receptors bind to the same population of binding sites. We emphasize that while the extended master equation accounts for both bleached and unbleached receptors simultaneously, our

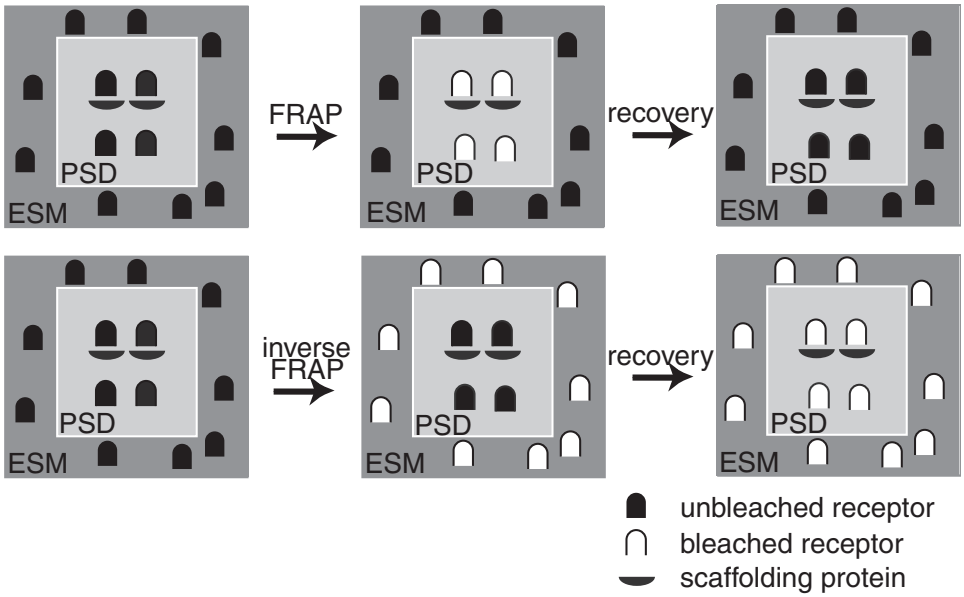

FIGURE 4 Schematic illustration of FRAP and inverse FRAP experiments. Here PSD is postsynaptic density, and ESM is extrasynaptic membrane. In a FRAP experiment, all receptors within the PSD are bleached at time $t = 0$, then the recovery of the unbleached receptors is observed thereafter. In an inverse FRAP experiment, all receptors outside of the PSD are bleached at time $t = 0$; the loss of unbleached receptors is observed thereafter.

analytical approximations can only account for one or the other receptor type separately. Nevertheless, we will show that in certain regimes our analytical results approximate the results obtained by Monte Carlo simulation of the extended master equation with high precision.

We mention that for each simulation in Fig. 5, the PSD is assumed to have a static gate with escape rate $\mu = 9.52\ s^{-1}$, although similar conclusions would be made using a stochastic gate. In Fig. 5, *A–C*, we plot the mean total number of receptors as a function of time during a FRAP-like simulation, meaning that initially there are neither free nor bound unbleached receptors ($n_0 = m_0 = 0$), but $C = 1$ so that the mean steady-state number of free unbleached receptors is one. (We note that the qualitative results of Fig. 5, *A–C*, are the same for any choice of $C > 0$.) The parameters L, α, and β are chosen differently in these figures, but always in a way so that the mean steady-state number of bound unbleached receptors is also one. In Fig. 5 *A*, we show results for a PSD in an unsaturated regime: $L = 100$, $\alpha = 10^{-2}\ s^{-1}$, and $\beta = 1\ s^{-1}$. In this case, our approximations for the mean and variance in the unsaturated regime, given in Eqs. 21 and 24, respectively, agree with the Monte Carlo simulation, because the PSD remains unsaturated during the entire simulation (i.e., $\alpha n(t) << \beta$). One may wonder why it is that our unsaturated approximation agrees with the Monte Carlo simulation if the Monte Carlo simulation accounts for both bleached and unbleached receptors but the unsaturated theory does not. The answer is that in the unsaturated regime the number of unoccupied binding sites is so large that unbound receptors do not compete with each other for them; i.e., the binding rates are nearly linear in the variables n and m, so the bleached and unbleached populations do not interact with each other. Fig. 5 *B* is similar to Fig. 5 *A* except $L = 1$, $\alpha = 1\ s^{-1}$, hence the PSD is neither saturated nor unsaturated. As one might expect, neither the mean nor variance of the saturated theory, given in Eqs. 31 and 33, respectively, nor those of the unsaturated theory approximate the mean and variance of the Monte Carlo simulation. Fig. 5 *C* is similar to Fig. 5 *B* except $\beta = 0.01\ s^{-1}$, hence the PSD is in a saturated regime. The Monte Carlo variance agrees with the saturated theory variance, as is expected, yet the means are very different. This is not unexpected, however, since our saturated approximation always assumes that all binding sites are occupied, yet in a FRAP simulation the number of bound receptors is initially zero (i.e., they have been bleached). This illustrates an important shortcoming of our saturated approximation: it is only valid when $m(t) \approx L$.

In Fig. 5, *D–F*, we show similar results for an inverse FRAP-like simulation. These figures are like Fig. 5, *A*, *B*, and *C*, respectively, except that for inverse FRAP we assume that initially there is one free and one bound receptor ($n_0 = m_0 = 1$), but $C = 0$ so that the mean steady-state number of free and bound receptors is zero. (We note that the qualitative results of Fig. 5, *D–F*, are the same for any choice of initial number of free and bound receptors.) When the PSD is in an unsaturated regime, our unsaturated theory agrees with the Monte Carlo simulation (see Fig. 5 *D*). In Fig. 5 *E*, we again consider a PSD that is neither saturated nor unsaturated. However, as bleached receptors leave the PSD during the course of the simulation, the PSD enters the unsaturated regime, and our unsaturated theory offers a good approximation in this case. In Fig. 5 *F*, a saturated PSD is again considered. Here the saturated theory offers a good approximation to the Monte Carlo simulation during the length of the simulation. Nevertheless, one can observe that near the end of the simulation the Monte Carlo mean begins to decrease as a result of the unbinding and escape of the bound receptor, while the saturated theory mean remains constant since the bound receptor never unbinds. Similarly, the Monte Carlo

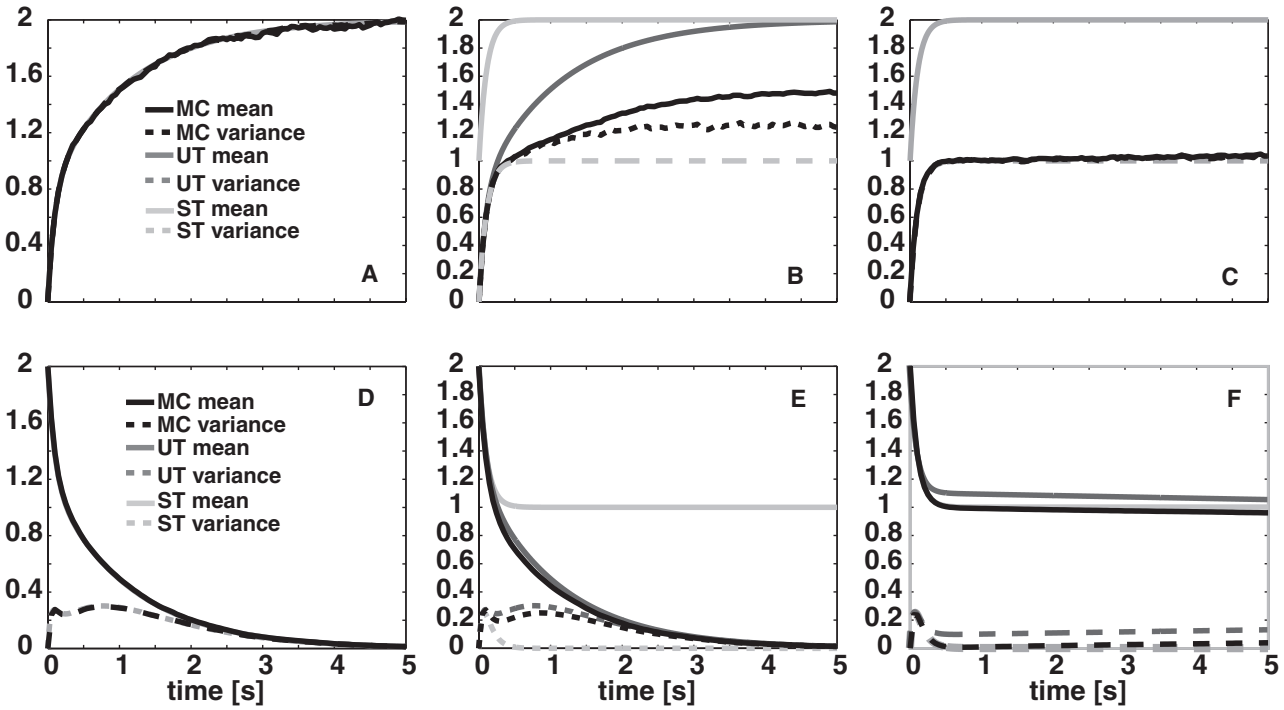

FIGURE 5 Comparison of saturated and unsaturated theory with Monte Carlo simulations. In all figures we assume PSD is static with $\mu = 9.52\ s^{-1}$. Similar results would be obtained with a dynamic gate. (*A–C*) Time-course of mean and variance of total receptor number during FRAP-like simulation. Initially there are no free or bound receptors ($n_0 = m_0 = 0$), but $C = 1$ so that the mean steady-state number of free receptors is one. The parameters L, α, and β are also chosen so that the mean steady-state number of bound receptors is one. (*A*) Here $L = 100$, $\alpha = 10^{-2}\ s^{-1}$, and $\beta = 1\ s^{-1}$, hence PSD is in an unsaturated regime. Monte Carlo simulation is equal to unsaturated theory (Eqs. 21 and 24). Note mean and variance of unsaturated theory are equal because the zero initial conditions yield a Poissonian process. (*B*) Similar to panel *A*, except $L = 1$, $\alpha = 1\ s^{-1}$, hence PSD is neither saturated nor unsaturated. Monte Carlo variance is between variances from saturated theory (Eqs. 31 and 33) and unsaturated theory. The mean from both regimes overestimates the Monte Carlo mean. (*C*) Similar to panel *B*, except $\beta = 0.01\ s^{-1}$, hence PSD is in a saturated regime. Monte Carlo variance and saturated theory variance are equal, but means are different since our saturated theory assumes all binding sites are occupied. (*D–F*) Time-course of mean and variance of total receptor number during inverse FRAP-like simulation. Initially there is one free and one bound receptor ($n_0 = m_0 = 1$), but $C = 0$, so that the mean steady-state number of free and bound receptors is zero. (*D*) Here $L = 100$, $\alpha = 10^{-2}\ s^{-1}$, and $\beta = 1\ s^{-1}$, hence PSD is in an unsaturated regime. Monte Carlo simulation and unsaturated theory agree. (*E*) Similar to panel *D*, except $L = 1$, $\alpha = 1\ s^{-1}$, hence PSD is neither saturated nor unsaturated. Unsaturated theory offers good approximation, especially as the number of receptors decreases and PSD transitions into an unsaturated regime. (*F*) Similar to panel *E*, except $\beta = 0.01\ s^{-1}$, hence PSD is in a saturated regime. The saturated theory approximates the Monte Carlo simulation well at first, but the approximation worsens near the end of the simulation since the bound receptor in the Monte Carlo simulation can unbind and escape, whereas it cannot in saturated theory.

variance increases near the end of the simulation while the saturated theory variance remains at zero.

Fig. 5 illustrates the fact that care must be taken when using the saturated regime approximation to infer the statistics of a saturated PSD, as the PSD may only be saturated during a portion of the simulation. Thus, in the following we will use our analytical calculations when considering the unsaturated regime but use Monte Carlo simulations when considering the saturated regime.

We now carry out in Figs. 6–8 a more detailed study of how receptor numbers relax to steady state during both FRAP and inverse FRAP simulations. To make comparisons with the dynamic corral model of Brown et al. (11), in each of these figures we take the gating parameters to be $\gamma_+ = 20\ s^{-1}$, $\gamma_- = 320\ s^{-1}$, and $\mu_o = 300\ s^{-1}$ for a stochastic gate and $\mu = 9.52\ s^{-1}$ for a static gate, as determined by Eq. 36. We want to systematically determine how the gating of the PSD in conjunction with the binding and unbinding of receptors within the PSD affect the outcome of FRAP and inverse FRAP simulations. Hence, in Figs. 6 and 7 we consider such simulations when the PSD is unsaturated and the binding and unbinding rates are, respectively, slow and comparable relative to the gating rates, and in Fig. 8 we consider a saturated PSD with binding and unbinding rates comparable to the gating rates. A summary of our results is given in Table 1.

In Fig. 6 we assume the PSD is unsaturated and that binding and unbinding are relatively slow compared to the dynamics of the gate: binding rate $\alpha = 10^{-3}\ s^{-1}$ and unbinding rate $\beta = 10^{-1}\ s^{-1}$, with number of binding sites $L = 100$. In Fig. 6, *A–C*, we plot the time course of the variance in total receptor numbers over 20 s using the unsaturated theory for different values of C (= 1, 5, and 10, respectively) during a FRAP-like experiment. Notice that here $\alpha L/\beta = 1$, so that the steady-state mean number of free and bound receptors is equal in each case. Also, since

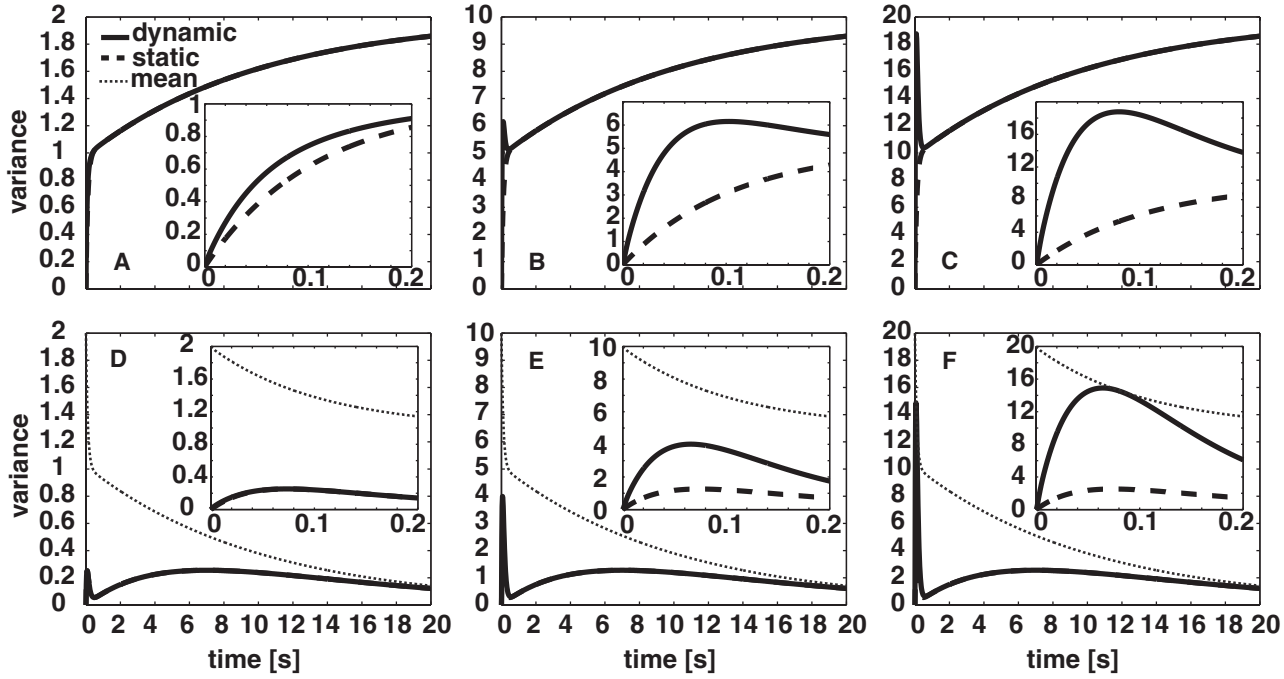

FIGURE 6 Time-course of mean and variance of total receptor numbers during FRAP- and inverse FRAP-like experiments for a dynamic (*solid*) and static (*dashed*) gate when the rates of binding and unbinding are slow compared to gate dynamics. We take $\alpha = 10^{-3}$ s^{-1}, $\beta = 10^{-1}$ s^{-1}, and $L = 100$. Gating parameters are taken to be $\gamma_+ = 20$ s^{-1}, $\gamma_- = 320$ s^{-1}, $\mu_o = 300$ s^{-1}, and $\mu = 9.52$ s^{-1} to compare with the work of Brown et al. (11). Plots constructed using Eqs. 19–24 for an unsaturated PSD. (*A–C*) FRAP-like simulations for $C = 1$, 5, and 10, respectively. The steady-state mean number of free and bound receptors is equal in each case as $\alpha L/\beta = 1$, and the mean and variance are equal throughout since the statistics are Poissonian. Compare the insets to Fig. 4 of Brown et al. (11). (*D–F*) Inverse FRAP-like simulations for initial conditions $n_0 = m_0 = 1$, 5, and 10, respectively. The mean is explicitly included (*dotted*). In panel *D*, the variances for both gates coincide. Compare the insets to Fig. 5 of Brown et al. (11).

there are initially no receptors, the statistics are Poissonian, implying that the mean and variance are equal throughout. The inset of each figure shows the first 0.2 s of each time course, and comparing these with Fig. 4 of Brown et al. (11), we see that the two models agree very well over this initial time interval. This is because we have taken binding to be slow relative to the opening and closing of the gate and to the entry of receptors through the gate, so that initially the mean/variance is dominated by free receptors entering the PSD. If there were no binding, our plots would approach a steady-state mean/variance of C free receptors in the same manner as Brown et al. (11). However, after ~0.5 s, the mean/variance begins to increase slowly toward C free and C bound receptors as free receptors bind to unoccupied binding sites. Notice also how in each figure except Fig. 6 *A* the variance is much larger for the stochastic PSD than for the static one during an initial transient. These observations suggest how an experimentalist might use FRAP to detect the presence of binding sites and/or a stochastic gate from a single set of experiments: the existence of two distinct timescales suggests the presence of a process like relatively slow binding/unbinding, and a large transient rise in the initial time-course of the variance suggests the presence of a stochastic gate.

In Fig. 6, *D–F*, we plot similar time courses for an inverse FRAP-like experiment where initially there are equal numbers of free and bound receptors, but in steady state there are $C = 0$ receptors. Comparing the insets to Fig. 5 of Brown et al. (11), we again find excellent agreement over short timescales due to the initial dominance of the dynamics by free receptors exiting the PSD. However, over longer times we observe a slow rise and fall in the variance due to the unbinding of bound receptors. As with the FRAP-like figures, in each case except for Fig. 6 *D*, the initial transient rise in variance is much larger for the stochastic PSD than for the static one. Hence it is clear that, using a set of inverse FRAP experiments, inferences could be made about the presence of binding/unbinding or a stochastic gate in a manner similar to that outlined in the previous paragraph for FRAP experiments.

Fig. 7 is similar to Fig. 6 except that now we choose binding and unbinding rates comparable to the dynamics of the gate: $\alpha = 1$ s^{-1}, $\beta = 100$ s^{-1}. As before, Fig. 7, *A–C*, are FRAP-like so that initially there are no receptors and in steady state there are C free and C bound receptors, and Fig. 7, *D–F*, are inverse FRAP-like so that initially there are equal numbers of free and bound receptors and no receptors in steady state. To illustrate further the effect that binding has on the mean and variance, we plot in shading the mean and variance when there is no binding. To make this comparison meaningful, in Fig. 7, *A–C*, we assume that in steady state there are $2C$ free receptors and in

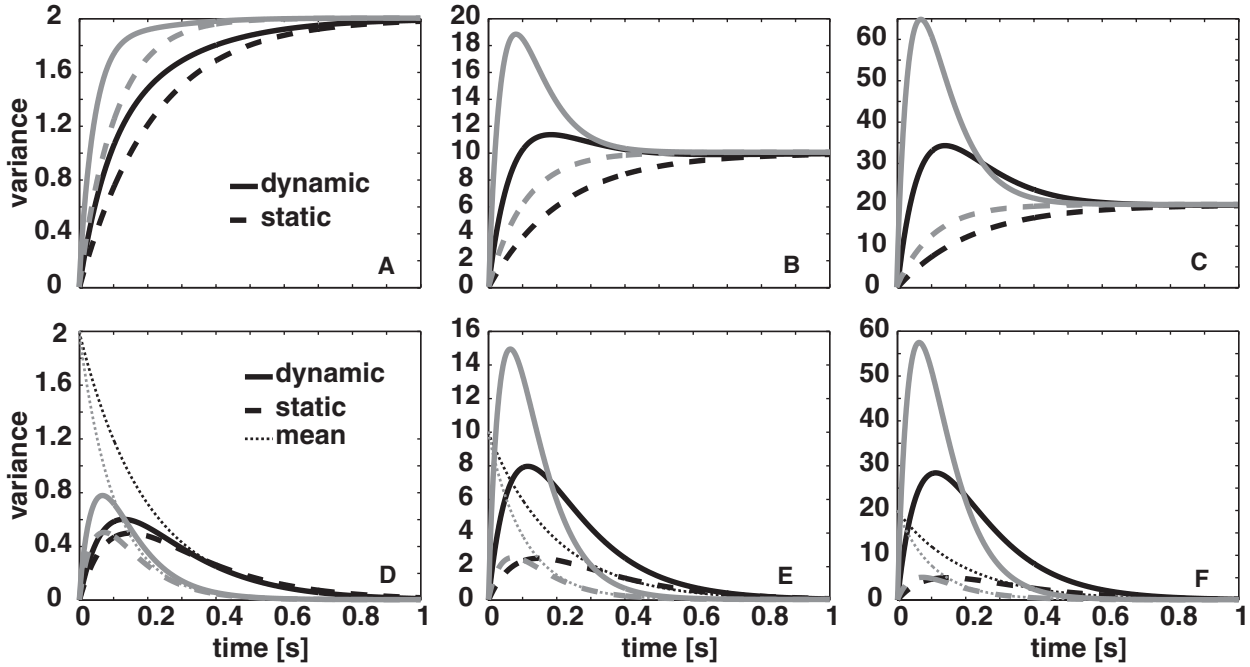

FIGURE 7 Similar to Fig. 6, except the rates of binding and unbinding are taken comparable to the dynamics of the gate: $\alpha = 1\ s^{-1}$, $\beta = 100\ s^{-1}$. Simulations without binding are also included (*shaded*) and assume $C = 2$, 10, and 20 in the FRAP-like simulations, for panels *A–C*; and $n_0 = 2$, 10, and 20, with $m_0 = 0$, in the inverse FRAP-like simulations in panels *D–F*.

Fig. 7, *D–F*, there are initially twice as many free receptors. Notice that for both kinds of experiments and especially in the case of a stochastic gate, fast binding/unbinding suppresses the transient rise in variance. This is due to two facts: 1), there is a great deal of variance arising from free receptors entering and exiting the stochastic gate; and 2), when binding is fast, free receptors quickly become bound after entering the PSD, minimizing their contribution to the variance. Such a tempering of the variance could indicate the presence of fast binding sites when the PSD is also stochastically gated. In the presence of a static gate, however, this tempering is not obvious in either of the two experiments, and so such an inference is not well justified.

Of course, any such inference is based on the assumption that the PSD is in an unsaturated regime. In Fig. 8, we show plots similar to those in Figs. 6 and 7, except now we assume that the PSD is saturated: $\alpha = 100\ s^{-1}$, $\beta = 1\ s^{-1}$, and the number of binding sites L is small ($L = 1$ in Fig. 8, *A* and *D*; $L = 5$ in Fig. 8, *B* and *E*; and $L = 10$ in Fig. 8, *C* and *F*). We note that, as was seen in Fig. 5, our saturated theory is not valid during the entire duration of either a FRAP or inverse FRAP experiment, and so the plots in Fig. 8 were obtained directly from Monte Carlo simulations of the extended master equation, Eq. 5. One immediately sees a difference between the saturated and unsaturated regimes in the FRAP-like experiments, since the steady-state variance in the saturated regime is only half that observed in the unsaturated regime (compare Fig. 8, *A–C*, with Fig. 6, *A–C*, or Fig. 7, *A–C*). This is because in the saturated regime only free receptors contribute to the steady-state variance. However, in the inverse FRAP experiments the difference in regimes is not at all apparent. In fact, Fig. 8, *D–F*, looks strikingly similar to Fig. 6, *D–F*, where unbinding was taken to be slow. Although the unbinding rates in these two sets of figures differ by an order of magnitude, the saturated regime makes unbinding effectively slow since free receptors are quick to bind available binding sites. Thus, one cannot easily distinguish between saturated and unsaturated regimes using inverse FRAP data alone, although the presence of a binding/unbinding-like process can again be inferred from the existence of two distinct timescales. As for the presence of a stochastic gate, one can again detect it in the large initial transient rise in variance, but this is obvious only in Fig. 8, *C*, *E*, and *F*, whereas, in Fig. 8 *B*, it is only slightly apparent.

DISCUSSION

In this article, we analyzed a simple stochastic model of receptor trafficking at a synapse in which both intrinsic and extrinsic sources of noise were included. Our model can be considered as an extension of two related models: 1), our model extended the receptor trafficking model of Holcman and Triller (10) by treating the PSD as stochastically gated, which provided our model with a generic source of extrinsic noise; and 2), our model extended the dynamic corral model of Brown et al. (11) by including binding sites within the corral. Combining analytical solutions of the master equation, Eq. 5, with Monte Carlo simulations, we

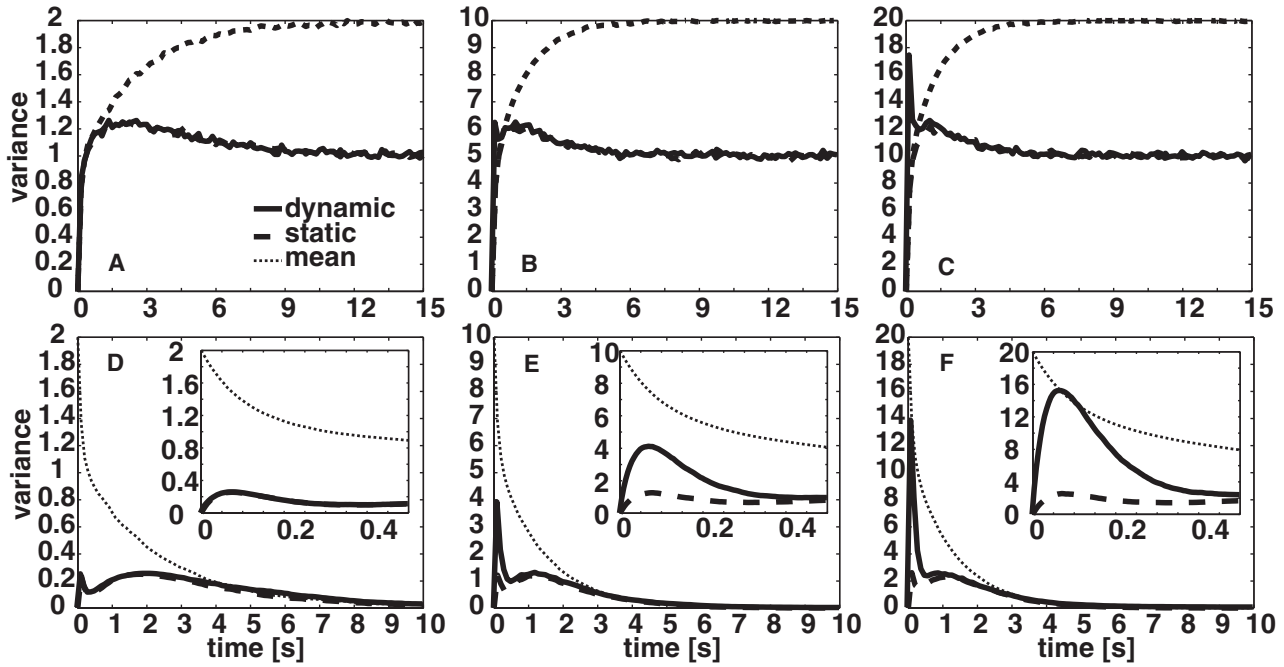

FIGURE 8 Similar to Fig. 6, except that the PSD is saturated: $\alpha = 100\ s^{-1}$, $\beta = 1\ s^{-1}$, $L = 1$ in panels *A* and *D*, $L = 5$ in panels *B* and *E*, and $L = 10$ in panels *C* and *F*. Plots constructed using Monte Carlo simulations of an extension of the master Eq. 5 which includes both bleached and unbleached receptors, as these compete with each other for binding sites in the saturated regime.

determined the steady-state and time-dependent behavior of the mean and variance of both free and bound receptor numbers under a variety of parameter regimes and initial conditions. Our purpose in doing this was to provide insight into how both intrinsic aspects (small receptor numbers, binding/unbinding) and extrinsic aspects (stochastic switching of the entry/exit rate) of receptor trafficking contribute to fluctuations in receptor number. By simulating FRAP and inverse FRAP-like experiments, we found that intrinsic and extrinsic sources of noise contribute differentially to these fluctuations, often with distinct signatures. Additionally, we showed that the relative contributions of intrinsic and extrinsic noise vary, depending upon whether the PSD is stochastically or statically gated; the PSD is in a saturated or unsaturated regime; and upon the type of experiment (e.g., FRAP or inverse FRAP) one is performing.

An important issue in cellular neuroscience is understanding how various sources of noise at a synapse influence information transmission and induce variability (37). One well-known manifestation of synaptic noise is the spontaneous miniature postsynaptic current (mPSC) that can be generated in the absence of any presynaptic input. The existence of mPSCs reflects the stochastic nature of neurotransmitter vesicle release, and establishes the quantal nature of synaptic transmission (38). There is also a trial-to-trial variability in the postsynaptic current evoked by the arrival of a single presynaptic action potential (39). In addition to the same stochastic processes that generate mPSCs, there are a number of other factors contributing to this variability. First, variability in the width of an action potential due to axonal channel noise can influence both the number of vesicles released and the probability of release (40). Second, there is randomness associated with the diffusion of neurotransmitter across the synaptic cleft and the subsequent binding to a fixed distribution of postsynaptic receptors; the efficacy of binding to receptors will also depend on the location of vesicle release within the presynaptic membrane, which itself varies from trial to trial (41). Third, receptor channel noise can also increase variability, particularly when the number of receptors is small. All of these mechanisms should influence variability in postsynaptic response sampled over relatively short timescales of seconds.

TABLE 1 Summary of FRAP and inverse FRAP results shown in Figs. 6–8

	Unsaturated PSD, binding << gating (Fig. 6)	Unsaturated PSD, binding ~ gating (Fig. 7)	Saturated PSD, binding ~ gating (Fig. 8)
Static gate	Two timescales, no initial transient in variance, variance = mean*	One timescale, no initial transient in variance, variance = mean*	Two timescales, no initial transient in variance, variance < mean*
Stochastic gate	Two timescales, initial transient in variance, variance = mean*	One timescale, suppressed initial transient in variance, variance = mean*	Two timescales, initial transient in variance, variance < mean*

*Relationship between the mean and variance only apply to FRAP.

One of the major implications of our current study (see also (10)) is that there is another potentially important source of synaptic noise, namely fluctuations in the number of synaptic receptors, which may manifest itself on the longer timescale of minutes rather than seconds. The variability in synaptic receptor number is illustrated by the individual trajectories shown in Fig. 3. In this article, we focused on how this variability might influence the fluorescent signal in FRAP experiments, for example, and what that might indicate about the structure of the PSD. However, it is clear that fluctuations in receptor number will also contribute to the trial-to-trial variability in the postsynaptic response to an action potential. In fact, a recent study (42) showed that immobilizing AMPA receptors reduced the coefficient of variation in evoked excitatory postsynaptic currents, a phenomenon usually attributed to presynaptic mechanisms. Stochastic models like ours could help in understanding how receptor trafficking contributes to such changes in variability. Note, however, that in estimating the size of such a contribution one cannot simply take the size of the evoked postsynaptic current to be proportional to the number of synaptic receptors, since the receptors may differ in their channel properties and there may be additional nonlinear interactions between receptors (43). Fluctuations in receptor number could also have an impact on synaptic plasticity, for there is growing experimental evidence that the activity-dependent regulation of AMPA receptor trafficking, which results in changes in the number of receptors within the PSD, is a major expression mechanism for modifying the strength of glutamatergic synapses (8,9). As an example, the same study (42) showed that the recovery of evoked excitatory postsynaptic currents after postsynaptic depression is due in part to the rapid exchange of desensitized synaptic AMPA receptors with naive, functional extrasynaptic AMPA receptors via lateral membrane diffusion. How intrinsic and extrinsic sources of receptor trafficking influence this exchange will be part of the focus of our future studies.

APPENDIX A

In this Appendix, we solve Eq. 7 for the generating function G defined in Eq. 6 with the initial condition $G(u,v,0) = u^{n_0}v^{m_0}$ via the method of characteristics (33). The associated set of characteristic equations are

$$\frac{du}{dt} = \mu(t)(u-1) + \alpha L(u-v),$$
$$\frac{dv}{dt} = -\beta(u-v),$$
$$\frac{dG}{dt} = \sigma(t)(u-1)G,$$

with initial conditions $u(U,V) = U$, $v(U,V) = V$, and $G(U,V) = U^{n_0}V^{m_0}$. Here U, V parameterize the corresponding set of characteristic curves. The solution for $u(t)$, $v(t)$ can be written in the matrix form

$$\begin{pmatrix} u(t)-1 \\ v(t)-1 \end{pmatrix} = N(t)^{-1}\begin{pmatrix} U-1 \\ V-1 \end{pmatrix}, \tag{37}$$

where

$$\mathcal{N}(t) = \exp\left(-\int_0^t N(t')dt'\right), \tag{38}$$

and

$$\mathcal{M}(t) = \begin{pmatrix} \mu(t)+\alpha L & -\alpha L \\ -\beta & \beta \end{pmatrix}. \tag{39}$$

Substituting $\sigma(t) = C\mu(t)$ into the characteristic equation for G, we find that

$$\frac{d\log G}{dt} = C\left(\frac{du}{dt} + \frac{\alpha L}{\beta}\frac{dv}{dt}\right),$$

which can be integrated to give

$$G = U^{n_0}V^{m_0}\exp\left(C(u(t)-U) + C\frac{\alpha L}{\beta}(v(t)-V)\right).$$

Inverting Eq. 37 to express the initial data U, V in terms of $u(t)$, $v(t)$ then gives, after some algebra, the solution given in Eq. 8.

APPENDIX B

In this Appendix, we calculate the averages $\langle \mathcal{N}_{ij}\rangle$ and $\langle \mathcal{N}_{ij}\mathcal{N}_{kl}\rangle$, where $\mathcal{N}_{ij}$ is the ij^{th} entry of the matrix $\mathcal{N}$ of Eq. 38. First, we introduce the stochastic dynamical system

$$\frac{d}{dt}\begin{pmatrix} x_1 \\ x_2 \end{pmatrix} = -\mathcal{M}(t)\begin{pmatrix} x_1 \\ x_2 \end{pmatrix}, \tag{40}$$

with $\mathcal{M}(t)$ defined in Eq. 39. Setting $\mathbf{x} = (x_1, x_2)^T$, $\mathbf{e}_1 = (1,0)^T$ and $\mathbf{e}_2 = (0,1)^T$, it follows that $\mathbf{x}(t) = \mathcal{M}(t)\mathbf{x}(0)$ and $x_i(t) = \mathcal{N}_{ij}(t)$ when $\mathbf{x}(0) = \mathbf{e}_j$. Next, we introduce the probability densities $\mathcal{P}_j^l$, $j = 1, 2$, $l = o, c$, defined as

$$\mathcal{P}_j^l(\mathbf{x},t)\mathrm{d}\mathbf{x} \equiv \mathrm{Prob}(\mathbf{x} \le \mathbf{x}(t) < \mathbf{x} + \mathrm{d}\mathbf{x}, \mu(t) = \mu_l)$$

with the initial conditions

$$\mathcal{P}_j^l(\mathbf{x},0) = \delta(\mathbf{x}-\mathbf{e}_j)\Pi_l.$$

Here δ is a Dirac delta function and Π_l, $l = o, c$, are the stationary probability distributions for the dichotomous noise process of Eq. 4:

$$\Pi_o = \frac{\gamma_+}{\gamma_+ + \gamma_-}, \quad \Pi_c = \frac{\gamma_-}{\gamma_+ + \gamma_-}.$$

The averages $\langle \mathcal{N}_{ij}\rangle$ and $\langle \mathcal{N}_{ik}\mathcal{N}_{jk}\rangle$ can then be determined in terms of first and second moments of the probability densities $\mathcal{P}_j^l$. That is,

$$\left\langle \mathcal{N}_{ij}(t)\right\rangle = m_{i,j}^o(t) + m_{i,j}^c(t)$$

and

$$\left\langle \mathcal{N}_{ik}(t)\mathcal{N}_{jk}(t)\right\rangle = m_{ij,k}^o(t) + m_{ij,k}^c(t),$$

where

$$m_{i,j}^l(t) = \int_{R^2} x_i\mathcal{P}_j^l(\mathbf{x},t)\mathrm{d}\mathbf{x} \quad (i,j = 1,2,\ l = o,c) \tag{41}$$

and

$$m_{ij,k}^l(t) = \int_{R^2} x_ix_j\mathcal{P}_k^l(\mathbf{x},t)\mathrm{d}\mathbf{x} \quad (i,j,k = 1,2,\ l = o,c). \tag{42}$$

To calculate these moments we derive a system of linear ordinary differential equations for them in the following manner. For $l = o, c$, let $\mathcal{M}_l$ denote the matrix obtained by setting $\mu(t) = \mu_l$ in Eq. 39. Given the underlying stochastic dynamical system Eq. 40, it follows from the theory of stochastic processes (33) that $\mathcal{P}_j^{\rm o}$ and $\mathcal{P}_j^{\rm c}$ evolve according to the master equation

$$\frac{\partial \mathcal{P}_j}{\partial t} = -\nabla \cdot \left[-\mathcal{M}_{\rm o}\mathbf{x}\mathcal{P}_j\right] - \gamma_-\mathcal{P}_j + \gamma_+\mathcal{P}_j$$

$$\frac{\partial \mathcal{P}_j}{\partial t} = -\nabla \cdot \left[-\mathcal{M}_{\rm c}\mathbf{x}\mathcal{P}_j\right] + \gamma_-\mathcal{P}_j - \gamma_+\mathcal{P}_j$$

or, expanding the divergences,

$$\frac{\partial \mathcal{P}_j^{\rm o}}{\partial t} = \frac{\partial}{\partial x_1}([(\mu_{\rm o} + \alpha L)x_1 - \alpha L x_2]\mathcal{P}_j^{\rm o}) - \beta\frac{\partial}{\partial x_2}([x_1 - x_2]\mathcal{P}_j^{\rm o}) - \gamma_-\mathcal{P}_j^{\rm o} + \gamma_+\mathcal{P}_j^{\rm c}, \quad (43)$$

$$\frac{\partial \mathcal{P}_j^{\rm c}}{\partial t} = \frac{\partial}{\partial x_1}([(\mu_{\rm c} + \alpha L)x_1 - \alpha L x_2]\mathcal{P}_j^{\rm c}) - \beta\frac{\partial}{\partial x_2}([x_1 - x_2]\mathcal{P}_j^{\rm c}) + \gamma_-\mathcal{P}_j^{\rm o} - \gamma_+\mathcal{P}_j^{\rm c}, \quad (44)$$

with the initial conditions $\mathcal{P}_j^l(\mathbf{x},0) = \delta(\mathbf{x} - \mathbf{e}_j)\Pi_l$. One interprets these equations as follows: at $\mathbf{x}$ the probability density $\mathcal{P}_j^l$ is advected with velocity $-\mathcal{M}_l\mathbf{x}$, as dictated by Eq. 40, while transitions between the open and closed distributions occur at rates $\gamma_\pm$. To calculate the first-order moments $m_{i,j}^l$ of Eq. 41, multiply both sides of Eqs. 43 and 44 by $x_{\rm i}$ and integrate with respect to $\mathbf{x}$. This leads to the matrix equation

$$\frac{d}{dt}\begin{pmatrix} m_{1,j}^{\rm o} \\ m_{1,j}^{\rm c} \\ m_{2,j}^{\rm o} \\ m_{2,j}^{\rm c} \end{pmatrix} = -\mathcal{Q}\begin{pmatrix} m_{1,j}^{\rm o} \\ m_{1,j}^{\rm c} \\ m_{2,j}^{\rm o} \\ m_{2,j}^{\rm c} \end{pmatrix}$$

with

$$\mathcal{Q} = \begin{pmatrix} \mu_{\rm o} + \alpha L + \gamma_- & -\gamma_+ & -\alpha L & 0 \\ -\gamma_- & \mu_{\rm c} + \alpha L + \gamma_+ & 0 & -\alpha L \\ -\beta & 0 & \beta + \gamma_- & -\gamma_+ \\ 0 & -\beta & -\gamma_- & \beta + \gamma_+ \end{pmatrix}$$

and initial conditions

$$m_{i,j}^l(0) = \begin{cases} \Pi_l, & i = j, \\ 0, & i \neq j. \end{cases}$$

Setting

$$\mathbf{q}^1 = (1,1,0,0), \mathbf{q}^2 = (0,0,1,1),$$

$$\mathbf{q}_1 = (\Pi_0, \Pi_{\rm c}, 0, 0)^T, \ \mathbf{q}_2 = (0,0,\Pi_0,\Pi_{\rm c})^T,$$

it follows that

$$\left\langle \mathcal{N}_{ij}(t) \right\rangle \equiv m_{i,j}^{\rm o}(t) + m_{i,j}^{\rm c}(t) = \mathbf{q}^i {\rm e}^{-\mathcal{Q}t}\mathbf{q}_j \quad (i,j = 1,2). \quad (45)$$

Similarly, the second-order moments $m_{ij,k}^l$ can be calculated by multiplying both sides of Eqs. 43 and 44 by $x_i x_j$ and integrating with respect to $\mathbf{x}$. This leads to the matrix equation

$$\frac{d}{dt}\begin{pmatrix} m_{11,k}^o \\ m_{11,k}^c \\ m_{12,k}^o \\ m_{12,k}^c \\ m_{22,k}^o \\ m_{22,k}^c \end{pmatrix} = -\mathcal{R}\begin{pmatrix} m_{11,k}^o \\ m_{11,k}^c \\ m_{12,k}^o \\ m_{12,k}^c \\ m_{22,k}^o \\ m_{22,k}^c \end{pmatrix},$$

where $\mathcal{R}$ is the 6×6 matrix

$$\mathcal{R} = \begin{pmatrix} \mathcal{J}_2(2\alpha L) & \mathcal{I}(2\alpha L) & \mathcal{I}(0) \\ \mathcal{I}(\beta) & \mathcal{J}_1(\alpha L + \beta) & \mathcal{I}(\alpha L) \\ \mathcal{I}(0) & \mathcal{I}(2\beta) & \mathcal{J}_0(2\beta) \end{pmatrix}$$

and we have introduced the 2×2 matrices

$$\mathcal{I}(a) = \begin{pmatrix} -a & 0 \\ 0 & -a \end{pmatrix},$$

$$\mathcal{J}_{\rm k}(a) = \begin{pmatrix} a + k\mu_{\rm o} + \gamma_- & -\gamma_+ \\ -\gamma_- & a + k\mu_{\rm c} + \gamma_+ \end{pmatrix}$$

for integers k. The initial conditions are

$$m_{ij,k}^l(0) = \begin{cases} \Pi_l, & i = j = k, \\ 0, & \text{else.} \end{cases}$$

Set

$$\mathbf{r}^{11} = (1,\ 1,\ 0,\ 0,\ 0,\ 0,),$$

$$\mathbf{r}^{12} = (0,\ 0,\ 1,\ 1,\ 0,\ 0,),$$

$$\mathbf{r}^{22} = (0,\ 0,\ 0,\ 0,\ 1,\ 1),$$

$$\mathbf{r}_1 = (\Pi_0,\ \Pi_c,\ 0,\ 0,\ 0,\ 0,)^T,$$

$$\mathbf{r}_2 = (0,\ 0,\ 0,\ 0,\ \Pi_0,\ \Pi_c)^T.$$

Then for $i, j, k = 1, 2$ with $i \leq j$, we have

$$\left\langle \mathcal{N}_{ik}(t)\mathcal{N}_{jk}(t) \right\rangle \equiv m_{ij,k}^{\rm o}(t) + m_{ij,k}^{\rm c}(t) = \mathbf{r}^{ij}{\rm e}^{-\mathcal{R}t}\mathbf{r}_k. \quad (46)$$

APPENDIX C

In this Appendix, we compute the averages $\langle \mathcal{N}_{i1}\mathcal{N}_{j2} \rangle$, which arise as part of the covariance of the free and bound particle numbers n and m (see Eq. 24). Unfortunately, they cannot be determined from moments of the probability densities $\mathcal{P}_j^l$ defined in Appendix B, since these do not express any codependence of n and m. (Roughly speaking, the index j, which indicates the initial condition $\mathbf{x}(0) = \mathbf{e}_{\rm j}$ for Eq. 40, tracks n-dependence when $j = 1$ and m-dependence when $j = 2$.) To proceed, therefore, we introduce the expanded stochastic dynamical system

$$\frac{d}{dt}\begin{pmatrix} x_1 \\ x_2 \\ y_1 \\ y_2 \end{pmatrix} = -\begin{pmatrix} \mathcal{M}(t) & 0 \\ 0 & \mathcal{M}(t) \end{pmatrix}\begin{pmatrix} x_1 \\ x_2 \\ y_1 \\ y_2 \end{pmatrix}, \quad (47)$$

with $\mathcal{M}(t)$ given by Eq. 39, and the joint probability densities

$$\mathcal{P}^l(\mathbf{x},\mathbf{y},t)\mathrm{d}\mathbf{x}\mathrm{d}\mathbf{y} = \mathrm{Prob}(\mathbf{x}\le\mathbf{x}(t)<\mathbf{x}+\mathrm{d}\mathbf{x}, \mathbf{y}\le\mathbf{y}(t)<\mathbf{y}+\mathrm{d}\mathbf{y}, \mu(t)=\mu_l)$$

subject to the initial conditions

$$\mathcal{P}^l(\mathbf{x},\mathbf{y},0) = \delta(\mathbf{x}-\mathbf{e}_1)\delta(\mathbf{y}-\mathbf{e}_2)\Pi_l.$$

It follows that $\mathbf{x}(t)=\mathcal{N}(t)\mathbf{x}(0)$ and $\mathbf{y}(t)=\mathcal{N}(t)\mathbf{y}(0)$, with $x_i(t)=\mathcal{N}_{i1}(t)$ and $y_i(t)=\mathcal{N}_{i2}(t)$ when $\mathbf{x}(0)=\mathbf{e}_1$ and $\mathbf{y}(0)=\mathbf{e}_2$. Defining the second moments

$$n_{ij}^l(t) = \int_{\mathrm{R}^2}\int_{\mathrm{R}^2} x_i y_j \mathcal{P}^l(\mathbf{x},\mathbf{y},t)\mathrm{d}\mathbf{x}\mathrm{d}\mathbf{y} \quad (i,j=1,2,\ l=\mathrm{o},\mathrm{c}), \tag{48}$$

we see that

$$\left\langle \mathcal{N}_{i1}(t)\mathcal{N}_{j2}(t)\right\rangle = n_{ij}^{\mathrm{o}}(t)+n_{ij}^{\mathrm{c}}(t).$$

Again, the moments can be calculated by solving a linear system of ordinary differential equations. The stochastic dynamical system given by Eq. 47 implies that P^l evolves according to the master equation

$$\frac{\partial\mathcal{P}^{\mathrm{o}}}{\partial t} = \nabla\cdot\left[\begin{pmatrix}\mathcal{M}_{\mathrm{o}}\mathbf{x}\\ \mathcal{M}_{\mathrm{o}}\mathbf{y}\end{pmatrix}\mathcal{P}^{\mathrm{o}}\right] - \gamma_-\mathcal{P}^{\mathrm{o}} + \gamma_+\mathcal{P}^{\mathrm{c}}, \tag{49}$$

$$\frac{\partial\mathcal{P}^{\mathrm{c}}}{\partial t} = \nabla\cdot\left[\begin{pmatrix}\mathcal{M}_{\mathrm{c}}\mathbf{x}\\ \mathcal{M}_{\mathrm{c}}\mathbf{y}\end{pmatrix}N^{\mathrm{c}}\right] + \gamma_-\mathcal{P}^{\mathrm{o}} - \gamma_+\mathcal{P}^{\mathrm{o}}, \tag{50}$$

where again $\mathcal{M}_l$ indicates the matrix obtained by setting $\mu(t)=\mu_l$ in Eq. 39. The initial conditions are

$$\mathcal{P}^l(\mathbf{x},\mathbf{y},0) = \delta(\mathbf{x}-\mathbf{e}_1)\delta(\mathbf{y}-\mathbf{e}_2)\Pi_l.$$

Multiplying both sides of Eqs. 49 and 50 by x_iy_j and integrating with respect to $\mathbf{x}$ and $\mathbf{y}$ leads to the matrix equation for the second-order moments n_{ij}^l of Eq. 48:

$$\frac{d}{dt}\begin{pmatrix}n_{11}^{\mathrm{o}}\\ n_{11}^{\mathrm{c}}\\ n_{12}^{\mathrm{o}}\\ n_{12}^{\mathrm{c}}\\ n_{21}^{\mathrm{o}}\\ n_{21}^{\mathrm{c}}\\ n_{22}^{\mathrm{o}}\\ n_{22}^{\mathrm{c}}\end{pmatrix} = -\mathcal{S}\begin{pmatrix}n_{11}^{\mathrm{o}}\\ n_{11}^{\mathrm{c}}\\ n_{12}^{\mathrm{o}}\\ n_{12}^{\mathrm{c}}\\ n_{21}^{\mathrm{o}}\\ n_{21}^{\mathrm{c}}\\ n_{22}^{\mathrm{o}}\\ n_{22}^{\mathrm{c}}\end{pmatrix},$$

where $\mathcal{S}$ is the 8×8 matrix

$$\mathcal{S} = \begin{pmatrix}\mathcal{J}_2(2\alpha L) & \mathcal{I}(\alpha L) & \mathcal{I}(\alpha L) & \mathcal{I}(0)\\ \mathcal{I}(\beta) & \mathcal{J}_1(\alpha L+\beta) & \mathcal{I}(0) & \mathcal{I}(\alpha L)\\ \mathcal{I}(\beta) & \mathcal{I}(0) & \mathcal{J}_1(\alpha L+\beta) & \mathcal{I}(\alpha L)\\ \mathcal{I}(0) & \mathcal{I}(\beta) & \mathcal{I}(\beta) & \mathcal{J}_0(2\beta)\end{pmatrix}.$$

The initial conditions are

$$n_{ij}^l(0) = \begin{cases}\Pi_l, & i=1, j=2,\\ 0, & \text{else.}\end{cases}$$

Letting

$$\mathbf{s}^{11} = (1,\ 1,\ 0,\ 0,\ 0,\ 0,\ 0,\ 0,),$$

$$\mathbf{s}^{12} = (0,\ 0,\ 1,\ 1,\ 0,\ 0,\ 0,\ 0),$$

$$\mathbf{s}^{21} = (0,0,0,\ 0,\ 1,\ 1,\ 0,\ 0),$$

$$\mathbf{s}^{22} = (0,\ 0,\ 0,\ 0,\ 0,\ 0,\ 1,\ 1),$$

$$\mathbf{s} = (0,\ 0,\ \Pi_0,\ \Pi_c,\ 0,\ 0,\ 0,0)^T,$$

we have

$$\left\langle \mathcal{N}_{i1}(t)\mathcal{N}_{j2}(t)\right\rangle \equiv n_{ij}^{\mathrm{o}}(t)+n_{ij}^{\mathrm{c}}(t) = \mathbf{s}^{ij}\mathrm{e}^{-St}\mathbf{s} \quad (i=1,2). \tag{51}$$

REFERENCES

1. Meier, J., C. Vannier, A. Serge, A. Triller, and D. Choquet. 2001. Fast and reversible trapping of surface glycine receptors by gephyrin. *Nat. Neurosci.* 4:253–260.
2. Borgdorff, A. J., and D. Choquet. 2002. Regulation of AMPA receptor lateral movements. *Nature*. 417:649–653.
3. Dahan, M., S. Levi, C. Luccardini, P. Rostaing, B. Riveau, et al. 2003. Diffusion dynamics of glycine receptors revealed by single-quantum dot tracking. *Science*. 302:442–445.
4. Groc, L., M. Heine, L. Cognet, K. Brickley, F. Stephenson, et al. 2004. Differential activity-dependent regulation of the lateral mobilities of AMPA and NMDA receptors. *Nat. Neurosci.* 7:695–696.
5. Ashby, M. C., S. R. Maier, A. Nishimune, and J. M. Henley. 2006. Lateral diffusion drives constitutive exchange of AMPA receptors at dendritic spines and is regulated by spine morphology. *J. Neurosci.* 26:7046–7055.
6. Ehlers, M. D., M. Heine, L. Groc, M.-C. Lee, and D. Choquet. 2007. Diffusional trapping of GluR1 AMPA receptors by input-specific synaptic activity. *Neuron*. 54:447–460.
7. Newpher, T. M., and M. D. Ehlers. 2008. Glutamate receptor dynamics in dendritic microdomains. *Neuron*. 58:472–497.
8. Bredt, D. S., and R. A. Nicoll. 2003. AMPA receptor trafficking at excitatory synapses. *Neuron*. 40:361–379.
9. Derkach, V. A., M. C. Oh, E. S. Guire, and T. R. Soderling. 2007. Regulatory mechanism of AMPA receptors in synaptic plasticity. *Nat. Rev. Neurosci.* 8:101–113.
10. Holcman, D., and A. Triller. 2006. Modeling synaptic dynamics driven by receptor lateral diffusion. *Biophys. J.* 91:2405–2415.
11. Brown, F. L. H., D. M. Leitner, J. A. McCammon, and K. R. Wilson. 2000. Lateral diffusion of membrane proteins in the presence of static and dynamic corrals: Suggestions for appropriate observables. *Biophys. J.* 78:2257–2269.
12. Leitner, D., F. Brown, and K. Wilson. 2000. Regulation of protein mobility in cell membranes: a dynamic corral model. *Biophys. J.* 78:125–135.
13. Saxton, M. J. 1993. Lateral diffusion in an archipelago. Single-particle diffusion. *Biophys. J.* 64:1766–1780.
14. Saxton, M. J. 1995. Single-particle tracking: effects of corrals. *Biophys. J.* 69:389–398.
15. Choquet, D., and A. Triller. 2003. The role of receptor diffusion in the organization of the postsynaptic membrane. *Nat. Rev. Neurosci.* 4:251–265.
16. Triller, A., and D. Choquet. 2005. Surface trafficking of receptors between synaptic and extrasynaptic membranes: and yet they do move!. *Trends Neurosci.* 28:133–139.

17. Holcman, D., and Z. Schuss. 2004. Escape through a small opening: receptor trafficking in a synaptic membrane. *J. Stat. Phys.* 117: 975–1014.

18. Taflia, A., and D. Holcman. 2007. Dwell time of a Brownian molecule in a microdomain with traps and a small hole on the boundary. *J. Chem. Phys.* 126:234107.

19. Chen, X., C. Winters, R. Azzam, X. Li, J. A. Galbraith, et al. 2008. Organization of the core structure of the postsynaptic density. *Proc. Natl. Acad. Sci. USA.* 105:4453–4458.

20. Ziff, E. B. 2007. Tarps and the AMPA receptor trafficking paradox. *Neuron.* 53:627–633.

21. Tomita, S., H. Adesnik, M. Sekiguchi, W. Zhang, K. Wada, et al. 2005. Stargazin modulates AMPA receptor gating and trafficking by distinct domains. *Nature.* 435:1052–1058.

22. Chen, L., D. Chetkovich, R. Petralia, N. Sweeney, Y. Kawasaki, et al. 2000. Stargazin regulates synaptic targeting of AMPA receptors by two distinct mechanisms. *Nature.* 408:936–943.

23. Luscher, C., H. Xia, E. Beattie, R. Carroll, M. von Zastrow, et al. 1999. Role of AMPA receptor cycling in synaptic transmission and plasticity. *Neuron.* 24:649–658.

24. Ehlers, M. 2000. Reinsertion or degradation of AMPA receptors determined by activity-dependent endocytic sorting. *Neuron.* 28:511–525.

25. Blanpied, T., D. Scott, and M. Ehlers. 2002. Dynamics and regulation of clathrin coats at specialized endocytic zones of dendrites and spines. *Neuron.* 36:435–449.

26. Kittler, J., P. Thomas, V. Tretter, Y. Bogdanov, V. Haucke, et al. 2004. Huntingtin-associated protein 1 regulates inhibitory synaptic transmission by modulating γ-aminobutyric acid type A receptor membrane trafficking. *Proc. Natl. Acad. Sci. USA.* 101:12736–12741.

27. Jacob, T. C., S. J. Moss, and R. Jurd. 2008. GABAA receptor trafficking and its role in the dynamic modulation of neuronal inhibition. *Nat. Rev. Neurosci.* 9:331–343.

28. Passafaro, M., V. Piech, and M. Sheng. 2001. Subunit-specific temporal and spatial patterns of AMPA receptor exocytosis in hippocampal neurons. *Nat. Neurosci.* 4:917–926.

29. Gerges, N. Z., D. S. Backos, C. N. Rupasinghe, M. R. Spaller, and J. A. Esteban. 2006. Dual role of the exocyst in AMPA receptor targeting and insertion into the postsynaptic membrane. *EMBO J.* 25: 1623–1634.

30. Earnshaw, B. A., and P. C. Bressloff. 2008. Modeling the role of lateral membrane diffusion in AMPA receptor trafficking along a spiny dendrite. *J. Comput. Neurosci.* 25:366–389.

31. Earnshaw, B. A., and P. C. Bressloff. 2006. Biophysical model of AMPA receptor trafficking and its regulation during long-term potentiation/long-term depression. *J. Neurosci.* 26:12362–12373.

32. Tanaka, J., M. Matsuzaki, E. Tarusawa, A. Momiyama, E. Molnar, et al. 2005. Number and density of AMPA receptors in single synapses in immature cerebellum. *J. Neurosci.* 25:799–807.

33. Kampen, N. G. V. 1992. Stochastic Processes in Physics and Biology, 2nd Ed. North-Holland, Amsterdam, The Netherlands.

34. Kubo, R. 1962. Stochastic theory of line-shape. *In* Fluctuation, Relaxation and Resonance in Magnetic Systems. D. TerHaar, editor. Oliver and Boyd, Edinburgh.

35. Zwanzig, R. 1990. Rate processes with dynamical disorder. *Acc. Chem. Res.* 23:148–152.

36. Gillespie, D. T. 1977. Exact stochastic simulation of coupled chemical reactions. *J. Phys. Chem.* 81:2340–2361.

37. Faisal, A. A., L. P. J. Selen, and D. M. Wolpert. 2008. Noise in the nervous system. *Nat. Rev. Neurosci.* 9:292–303.

38. Fatt, P., and B. Katz. 1950. Some observations on biological noise. *Nature.* 166:597–598.

39. Bekkers, J. M., G. B. Richerson, and C. F. Stevens. 1990. Origin of variability in quantal size in cultured hippocampal neurons and hippocampal slices. *Proc. Natl. Acad. Sci. USA.* 87:5359–5362.

40. Faisal, A. A., and S. B. Laughlin. 2007. Stochastic simulations on the reliability of action potential propagation in thin axons. *PLoS Comput. Biol.* 3:e79.

41. Franks, K. M., C. F. Stevens, and T. J. Sejnowski. 2003. Independent sources of quantal variability at single glutamatergic synapses. *J. Neurosci.* 23:3186–3195.

42. Heine, M., L. Groc, R. Frischknecht, J.-C. Beique, B. Lounis, et al. 2008. Surface mobility of postsynaptic AMPARs tunes synaptic transmission. *Science.* 320:201–205.

43. Holmes, W. R., and L. M. Grover. 2006. Quantifying the magnitude of changes in synaptic level parameters with long-term potentiation. *J. Neurophysiol.* 96:1478–1491.